

Journal Pre-proof

Functional diversification within the heme-binding split-barrel family

Nicolas Grosjean, Lifang Zhang, Desigan Kumaran, Meng Xie, Audrey Fahey, Kassandra Santiago, Fangle Hu, Michael Regulski, Ian K. Blaby, Doreen Ware, Crysten E. Blaby-Haas

PII: S0021-9258(24)02390-1

DOI: <https://doi.org/10.1016/j.jbc.2024.107888>

Reference: JBC 107888

To appear in: *Journal of Biological Chemistry*

Received Date: 14 May 2024

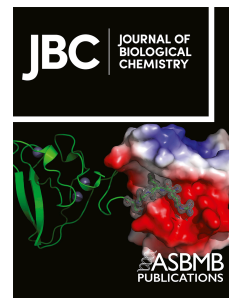
Revised Date: 29 September 2024

Accepted Date: 7 October 2024

Please cite this article as: Grosjean N, Zhang L, Kumaran D, Xie M, Fahey A, Santiago K, Hu F, Regulski M, Blaby IK, Ware D, Blaby-Haas CE, Functional diversification within the heme-binding split-barrel family, *Journal of Biological Chemistry* (2024), doi: <https://doi.org/10.1016/j.jbc.2024.107888>.

This is a PDF file of an article that has undergone enhancements after acceptance, such as the addition of a cover page and metadata, and formatting for readability, but it is not yet the definitive version of record. This version will undergo additional copyediting, typesetting and review before it is published in its final form, but we are providing this version to give early visibility of the article. Please note that, during the production process, errors may be discovered which could affect the content, and all legal disclaimers that apply to the journal pertain.

© 2024 THE AUTHORS. Published by Elsevier Inc on behalf of American Society for Biochemistry and Molecular Biology.



1 Functional diversification within the heme-binding split-barrel family

2
3 Nicolas Grosjean^{1,#,\$}, Lifang Zhang^{2,\$}, Desigan Kumaran^{1,\$}, Meng Xie¹, Audrey Fahey², Kassandra
4 Santiago¹, Fangle Hu², Michael Regulski², Ian K. Blaby³, Doreen Ware^{2,4*}, Crysten E. Blaby-Haas^{3,5*}

5
6 ¹ Biology Department, Brookhaven National Laboratory, Upton, NY, 11973, USA

7 ² Cold Spring Harbor Laboratory, Cold Spring Harbor, NY, 11724, USA

8 ³ US Department of Energy Joint Genome Institute, Lawrence Berkeley National Laboratory, Berkeley,
9 CA, 94720, USA

10 ⁴ USDA ARS NEA Plant, Soil & Nutrition Laboratory Research Unit, Ithaca, NY, 14853, USA

11 ⁵ The Molecular Foundry, Lawrence Berkeley National Laboratory, Berkeley, CA, USA

12 # present affiliation: US Department of Energy Joint Genome Institute, Lawrence Berkeley National
13 Laboratory, Berkeley, CA, 94720, USA

14 \$these authors contributed equally

15 [*ware@cshl.edu](mailto:ware@cshl.edu)

16 [*cblaby@lbl.gov](mailto:cblaby@lbl.gov)

17
18
19 Running title: Heme-binding split-barrel family in plants

20
21 Keywords: iron, chloroplast, AT3G03890, HOZ, AT1G51560, HOZ2A, AT3G21140, HOZ2B, GluTRBP

22
23
24 **Abstract**

25 Due to neofunctionalization, a single fold can be identified in multiple proteins that have distinct molecular
26 functions. Depending on the time that has passed since gene duplication and the number of mutations, the
27 sequence similarity between functionally divergent proteins can be relatively high, eroding the value of
28 sequence similarity as the sole tool for accurately annotating the function of uncharacterized homologs.
29 Here, we combine bioinformatic approaches with targeted experimentation to reveal a large multi-
30 functional family of putative enzymatic and non-enzymatic proteins involved in heme metabolism. This
31 family (homolog of HugZ (HOZ)) is embedded in the “FMN-binding split barrel” superfamily and contains
32 separate groups of proteins from prokaryotes, plants, and algae, which bind heme and either catalyze its
33 degradation or function as non-enzymatic heme sensors. In prokaryotes these proteins are often involved in
34 iron assimilation, whereas several plant and algal homologs are predicted to degrade heme in the plastid or
35 regulate heme biosynthesis. In the plant *Arabidopsis thaliana*, which contains two HOZ subfamilies that
36 can degrade heme *in vitro* (HOZ1 and HOZ2), disruption of *AtHOZ1* (AT3G03890) or *AtHOZ2A*
37 (AT1G51560) causes developmental delays, pointing to important biological roles in the plastid. In the tree
38 *Populus trichocarpa*, a recent duplication event of a *HOZ1* ancestor has resulted in localization of a paralog
39 to the cytosol. Structural characterization of this cytosolic paralog and comparison to published homologous
40 structures suggests conservation of heme-binding sites. This study unifies our understanding of the
41 sequence-structure-function relationships within this multi-lineage family of heme-binding proteins and
42 presents new molecular players in plant and bacterial heme metabolism.

52 Introduction

53
54 Iron is an essential micronutrient that functions in a wide range of biological processes. To control the
55 chemical properties of the iron atom and catalyze a specific activity, multiple proteins and complexes bind
56 a prosthetic group where iron is bound to a protoporphyrin ring (*i.e.*, heme). The specific interactions
57 between heme and the polypeptide tailors the function of the iron atom, such as tuning the redox potential
58 or enabling oxygen transport. While the malleable function of heme has resulted in its use by a plethora of
59 proteins, free heme can be highly toxic (1). As an example, the plant plastid has an absolute requirement
60 for heme in many of the electron transfer reactions during photosynthesis, but free heme can react with
61 lipoproteins and oxygen species leading to membrane and protein damage (2). As such, heme biosynthesis,
62 availability, and turnover must be tightly regulated.

63
64 Enzymatic degradation to detoxify free heme and recycle the iron atom usually involves oxidative cleavage
65 by a heme oxygenase. This enzymatic activity is proposed to have evolved at least three independent times.
66 Once with the canonical heme oxygenases (*i.e.*, HO from mammals, HMX1 from yeast, and HmuO from
67 *Corynebacterium diphtheriae*), which compose a family of proteins that share an overall α -helical structural
68 fold (3, 4). At another time, heme oxygenases evolved from within the dimeric alpha-beta barrel
69 superfamily (*i.e.*, IsdG and IsdI from *Staphylococcus aureus* (5, 6) and LFO1 from *Chlamydomonas*
70 *reinhardtii* (7)) and are related to the antibiotic biosynthesis monooxygenases (ABM) (6). The third
71 example of convergent evolution includes the proposed heme-degradation proteins from the “FMN-binding
72 split barrel” superfamily (*i.e.*, HugZ from *Helicobacter pylori*, HutZ from *Vibrio cholerae*, and HOZ from
73 *Arabidopsis thaliana*) (8–10).

74
75 This latter superfamily, “FMN-binding split barrel”, comprises a collection of structurally similar proteins,
76 which was named based on an FMN-binding protein of unknown biological function from *Desulfovibrio*
77 *vulgaris* (11). Although some family members, such as pyridoxine 5'-phosphate oxidase and a ferric
78 reductase from *Archaeoglobus fulgidus* (locus: AF_0830), have been found to bind FMN, many members
79 do not, such as the heme-degradation proteins. Therefore, the name “FMN-binding split barrel” can be a
80 source of confusion and has led to an unfortunate instance of mis-annotation when membership in this
81 family is used to infer FMN binding. The superfamily has also been named flavin (FMN/FAD)/deazaflavin
82 (F₄₂₀) oxidoreductases (FDOR) based on studies of a large group of related enzymes in mycobacteria and
83 elsewhere (12), but, again, a number of family members do not bind either cofactor, nor do all family
84 members function as oxidoreductases. Additionally, multiple members of the split-barrel superfamily
85 contain an array of domains fused to the common split-barrel fold, such as the bifunctional
86 epimerase/oxidase PDX3 in plants (13). Other family members, such as human CREG (14) and plant
87 GluTRBP/GBP (15, 16) have no known enzymatic activity and, instead, function as regulators. Herein, we
88 refer to this superfamily as the “split-barrel superfamily” to avoid presumption of function due to
89 superfamily membership. Further, we refer to the heme-binding subfamily as the “heme-binding split-barrel
90 family” for inclusion of proteins that function as enzymes or regulators.

91
92 The putative heme-degradation enzymes from the heme-binding split-barrel family have been found to have
93 different substrates and products. HugZ from *Helicobacter pylori* can bind hemin and produce biliverdin
94 IX δ in the presence of a reductant (17), while, for HutZ from *Vibrio cholerae*, the cleavage site is in the β -
95 or δ -meso position (18). Diverging from these homologs, Pden_1323 from *Paracoccus denitrificans*
96 cleaves *c*-type hemopeptides producing peptide-linked biliverdin (19), while HupZ from *Streptococcus*
97 *pyogenes* is proposed to function as a heme chaperone (20). Analogous to HugZ and HutZ, the plant
98 homolog HOZ is also capable of degrading heme to biliverdin *in vitro* (8), but while these bacterial proteins
99 are involved in heme utilization, the biological function of HOZ in plants is unknown.

100
101 Here, we combine sequence and structure analyses with *in vitro* and *in vivo* experimentation to better
102 understand the evolution and presence of heme-degradation activity among the split-barrel superfamily,

103 with a focus on plant homologs. We identify several distinct families of putative heme-binding proteins
 104 across plants, algae, fungi, and prokaryotes. Using a yeast-based complementation assay, we identify two
 105 *A. thaliana* family members: the recently described plastidial heme-degradation protein HOZ (renamed
 106 HOZ1) from *A. thaliana* (8) and a paralog that we have named *HOZ2A*, which rescue loss of the *HMX1*
 107 gene in *Saccharomyces cerevisiae*. Using CRISPR-Cas to generate loss-of-function mutants in *HOZ1* and
 108 a T-DNA insertion line for *HOZ2A*, we find that *HOZ1* and *HOZ2A* are important for plant development.
 109 Using structural and biochemical characterization of *HOZ1* orthologs from taxonomically diverse plants,
 110 we find that heme-degradation activity is conserved in grasses (represented by *Sorghum bicolor*) and trees
 111 (represented by *Populus trichocarpa*). A gene duplication event in a *Saliceae* ancestor followed by loss of
 112 the transit peptide resulted in the presence of a HOZ1 paralog in the cytosol of *P. trichocarpa*, in addition
 113 to retention of the ancestral plastidial enzyme. A crystal structure of the cytosolic poplar HOZ1-like protein
 114 suggests conservation of the heme-binding sites observed in bacterial proteins HugZ, ChuZ, and AtHOZ1.
 115

116 Results

117 Phylogenomic analysis of the split-barrel family in plants and algae

118 Although commonly annotated based on their similarity to pyridoxamine 5'-phosphate oxidase (often
 119 abbreviated to PNPO or PPO), plant and algal members of the split-barrel family belong to multiple distinct
 120 subfamilies (Figure 1). Domain analysis combined with phylogenetic reconstruction encompassing
 121 prokaryotic homologs further supports similarity among members of individual subfamilies and divergence
 122 between subfamilies (Figure 2). Across the split-barrel family, three groups of plant proteins also contain
 123 the recently named Domain Related to Iron (DRI) found in the bacterial heme-utilization proteins, HugZ
 124 (10) and ChuZ (21), and in the heme-binding protein Dri1 from cyanobacteria (22) (Figures 1 and 2). Of
 125 the DRI-containing *A. thaliana* proteins, GBP (GluTR Binding Protein) orthologs form a sequence
 126 similarity cluster with two additional subclusters (Figure 1). Based on phylogeny of the split-barrel domain
 127 sequences, these proteins form three distinct clades (Figure 2F). One subfamily, which we have renamed
 128 HOZ1, contains the previously described HOZ protein from *A. thaliana* (8) and other uncharacterized plant
 129 and algal proteins. The second subfamily, which we have named HOZ2, contains uncharacterized plant and
 130 algal proteins. Given the phylogenetic relatedness between these eukaryotic split-barrel domain proteins,
 131 we refer to this subfamily of the heme-binding split-barrel family (*i.e.*, HOZ1, HOZ2, and GBP) as HOZ
 132 (Figure 2F).
 133

134 The HOZ family is related to a large number of prokaryotic proteins. Like the *A. thaliana* HOZ family, the
 135 majority of prokaryotic proteins contain the split-barrel domain followed by DRI, which is opposite to the
 136 domain architecture in HugZ (Figure 2). To provide insight into the function of the plant HOZ family and
 137 related proteins, we analyzed the genomic context of the related prokaryotic homologs (Figure 3) (23). We
 138 identified three subfamilies of HOZ-like prokaryotic homologs that are commonly encoded by genes next
 139 to, and potentially sharing operons with, genes encoding proteins related to iron or heme transport and
 140 homeostasis, such as proteins similar to ferritin, transferrin, siderophore-interacting proteins, ChuX, HtaA,
 141 TonB-dependent receptors similar to CirA, and putative iron transporters from the NRAMP, BPD, and
 142 FecCD families (Figure 3B). These gene neighborhoods may represent heme-uptake and -utilization gene
 143 clusters. We also identified predicted protein fusions (in four separate species), represented by
 144 PAI11_25360 from *Patulibacter medicamentivorans*, involving a HOZ-like protein and an ABC-type
 145 periplasmic binding domain (Figure 3C). Specifically, the periplasmic binding protein region is similar to
 146 FepB and FhuD, which are periplasmic components of ABC-type Fe³⁺-siderophore transport systems.
 147 Combined, these bioinformatic analyses suggest that the ancestor of the plant HOZ family was involved in
 148 heme utilization and, as such, a role in heme degradation could be conserved among different
 149 uncharacterized members of the plant HOZ family.
 150

151 Yeast complementation suggests conservation and presence of a second HOZ-like heme-degradation 152 subfamily in plants

153 To determine whether heme-degradation activity may be conserved among these plant homologs, we
154 leveraged a yeast-based complementation assay. The *S. cerevisiae* genome encodes only one canonical
155 heme oxygenase, Hmx1p. Deletion of *HMX1* has been previously shown to result in H₂O₂ sensitivity (24).
156 Presumably, this sensitivity is at least partially due to the loss of enzymatic degradation of heme, a pro-
157 oxidant that subsequently accumulates in the mutant, and to the loss of bilirubin, an antioxidant formed
158 from the heme-degradation product biliverdin. Although, the exact mechanism of Hmx1p and/or its
159 degradation products in abating oxidative stress may be more complex (24). Since recombinantly produced
160 AtHOZ1 can degrade heme and produce biliverdin *in vitro* (8), we reasoned that expression of AtHOZ1
161 should be able to rescue the H₂O₂-sensitivity of the yeast *hmx1Δ* mutant, and that this strain and phenotype
162 can be used to screen for conservation of heme-degradation activity. Indeed, like expression of the yeast
163 *hmx1* gene *in trans*, AtHOZ1 can rescue the H₂O₂-dependent growth defect (Figure 4B). With the
164 complementation assay established, we screened the other HOZ family *A. thaliana* genes. Of the 7 other *A.*
165 *thaliana* proteins that contain DRI (Figure 2A), we only observed rescue by AtHOZ2A (AT1G51560),
166 suggesting that this closely related HOZ1-like subfamily also contains members that can degrade heme
167 (Figure 4B). However, we note that the paralog AtHOZ2B (AT3G21140) did not rescue the growth defect.
168

169 We also tested conservation of HOZ1 function across land plants and green algae. The HOZ1 family is
170 typically found as single-copy genes in plant and algal genomes, and predicted plastid-localization transit
171 peptides are generally conserved (Figure 4A). An exception is the tree *P. trichocarpa* (Figure 4A), where
172 there are two paralogs: one with a predicted plastid transit peptide (Potri.019G035200; PtHOZ1A) and one
173 predicted to localize to the cytosol (Potri.013G057700; PtHOZ1B). The presence of the putatively cytosolic
174 paralog suggests that neofunctionalization may have resulted in the evolution of HOZ1-catalyzed heme
175 degradation in the cytosol. To test this hypothesis, we performed localization experiments with the two *P.*
176 *trichocarpa* paralogs and the single ortholog from *S. bicolor*. As expected, based on the sequence analysis,
177 one *P. trichocarpa* paralog has retained the ancestral localization to the plastid, while the duplicated copy
178 has lost the transit peptide and localizes to the cytosol (Figure 5A-C). HOZ1 from *S. bicolor* localizes to
179 the chloroplast, as observed for PtHOZ1A and previously observed for AtHOZ1 (8), but was also found in
180 the nucleus, as has been observed for the canonical heme oxygenase in yeast and animals (25). Three
181 subcellular localization patterns of *S. bicolor* HOZ1 (Figure 5C) could suggest possible retrograde
182 translocation (26).
183

184 Expression of the AtHOZ1 ortholog from *S. bicolor* and the paralogs from *P. trichocarpa* rescued the H₂O₂-
185 sensitive phenotype, while the ortholog from the green alga *C. reinhardtii* failed to rescue, either because
186 of poor expression or functional divergence. However, we did observe *in vitro* that the recombinantly
187 produced *S. bicolor* and *P. trichocarpa* HOZ1 proteins could bind and degrade heme, while the algal protein
188 had relatively poor heme-binding and -degradation activities (Figure 5D-F). *In vitro*, the purified land plant
189 HOZ1 proteins displayed a characteristic Soret peak at 405 nm in the presence of heme, while the
190 characteristic shift from 385 nm to 405 nm in the UV-VIS spectra was far less obvious with the *C.*
191 *reinhardtii* ortholog (Figure 5D). To investigate whether the proteins are able to degrade heme, ascorbate
192 was added as an electron donor together with purified protein and heme, and spectral changes were collected
193 over time. As previously observed for AtHOZ1, there was noticeable reduction of the Soret peak for the
194 land plant proteins, indicative of their heme degradation ability *in vitro*, but this reduction was less obvious
195 with the *C. reinhardtii* protein (Figure 5F).
196

197 Although we could not find evidence of heme binding for the algal protein, the function of related bacterial
198 proteins in Fe- and heme-utilization suggests that these eukaryotic proteins could have similar biological
199 functions. We therefore tested whether the algal gene is required for growth in suboptimal iron availability
200 and when growth is dependent on photosynthesis (photoautotrophic growth). We did not observe a growth
201 defect when acetate (a reduced carbon source; TAP medium) is provided (Figure 5G), but a growth defect
202 was apparent during photoautotrophic growth (in the absence of acetate; TP medium) (Figure 5H and I),
203 which is consistent with a biological role of CrHOZ1 in chloroplast physiology. Under the conditions tested

204 in this study, the amount of iron in the medium did not appear to have a major impact on the *C. reinhardtii*
 205 mutant growth compared to WT (Figure 5H).

206

207 **AtHOZ1 and AtHOZ2A, but not AtHOZ2B, are important for development**

208 We generated mutant lines of *AtHOZ1* using CRISPR-Cas9 and acquired T-DNA lines of *AtHOZ2A* and
 209 *AtHOZ2B*. The resulting *AtHOZ1* mutants *hoz1-1* and *hoz1-3* contain 5 bp or 38 bp deletions, respectively,
 210 resulting in premature stop codons in both mutants (Figure S3). Compared to the parent, the *AtHOZ1* and
 211 *AtHOZ2A* mutants, but not the *AtHOZ2B* mutant, showed developmental delays when grown in soil
 212 (Figures 6 and S7). Given the experimentally determined location of *AtHOZ1* (8) and predicted location of
 213 *AtHOZ2A* in the plastid, these proteins appear to play important roles in chloroplast biology. Presumably,
 214 the function of *AtHOZ1* and *AtHOZ2A* are independent to some extent, and their roles cannot be performed
 215 by plastid-localized members of the canonical heme oxygenase family. The homozygous *hoz2a hoz2b*
 216 mutant is similar to the *hoz2a* mutant. The triple *hoz1-1 hoz2a hoz2b* mutant had a similar developmental
 217 delay to the *hoz1-1* and *hoz2a* mutants (Figures 6 and S7).

218

219 **Structure of the cytosolic poplar paralog**

220 PtHOZ1B, the recently evolved cytosolic version of HOZ1, was recombinantly expressed in *Escherichia*
 221 *coli*, purified using Ni-NTA affinity chromatography, and crystallized. The crystal structure of PtHOZ1B
 222 was determined to 1.8 Å resolution by the single wavelength anomalous dispersion (SAD) method. The
 223 crystal belonged to the tetragonal system, with space group $P4_22_12$ and contains one molecule per
 224 asymmetric unit (Table S1). As with the plastid-localized *AtHOZ1* (8), PtHOZ1B forms a dimer through a
 225 crystallographic two-fold symmetry via the split-barrel domains, with the DRI regions oriented away from
 226 the dimerization interface (Figure 7A and 7B). Unlike *AtHOZ1*, we were unable to acquire a crystal
 227 structure bound to heme. Additionally, the PtHOZ1B dimer is slightly more compact than *AtHOZ1* (Figure
 228 S4A), and four metal-binding sites are observed in the dimer, which have not been found in *AtHOZ1*
 229 (Figure 7B). Metal site 1A and 1B are at the dimer interface with residues from the split-barrel domains,
 230 while metal site 2A and 2B are in the DRI regions (Figure 7A). X-ray fluorescence energy scan (data not
 231 shown) of purified protein and crystals showed the presence of nickel ions (likely from the Ni-resin used
 232 for purification). Metal sites 1A and 1B have a distorted octahedral geometry formed by coordination with
 233 His61 and His90 of one subunit and His119 and Gln163 of another subunit (Figure S4B). The fifth
 234 coordination is from Glu279 of the intermolecularly interacting (symmetry related) molecule of subunit 1,
 235 and this coordinating side chain could be due to an effect of crystal packing (Figure S4B). A water molecule
 236 completes the coordination sphere (Figure S4B). Metal sites 2A and 2B consist of His201, His206 and four
 237 water molecules located at the surface of the DRI regions (Figure S4C).

238

239 Although we were unable to acquire a crystal structure of heme bound to PtHOZ1B, these metal-binding
 240 sites may be heme-binding sites based on structural homology with heme-bound crystal structures of HugZ,
 241 ChuZ and *AtHOZ1*. As observed previously (8), the heme bound at the dimer interface of HugZ and the
 242 heme bound at the dimer interface of *AtHOZ1* align well (Figure 7C and 7D). A conserved histidine residue,
 243 His135 in *AtHOZ1* and His136 in HugZ, interact with the propionic side chains (Figure 7D). This histidine
 244 residue is also conserved in PtHOZ1B (His90), but its side chain imidazole moiety is rotated, coordinating
 245 the metal ion found at the dimer interface (Figure 7D). To better understand whether these amino acid side
 246 chains may function in heme degradation by PtHOZ1B, we generated point mutations in metal binding site
 247 1 and in the predicted heme-binding pocket and tested their impact on the ability of the PtHOZ1B to rescue
 248 the H₂O₂ sensitivity of a *hmx1Δ* yeast strain. Unlike WT PtHOZ1B, mutants with mutated residues that line
 249 the predicted heme-binding pocket or are in metal site 1 could not rescue the H₂O₂-sensitivity of the *hmx1Δ*
 250 mutant (Figure S5).

251

252 Although not observed in *AtHOZ1* and HugZ, the crystal structure of ChuZ from *Campylobacter jejuni*
 253 contains an extra heme bound to the DRI region (21). This heme is referred to as “extra”, because it is an
 254 additional heme not previously observed in the HugZ structure from *H. pylori*. The extra heme of ChuZ

255 aligns well with the metal site 2 of PtHOZ1B, with the two heme-binding histidine residues of ChuZ
 256 aligning with the two metal-binding residues of PtHOZ1B (Figure 7E-G). Although there is no electron
 257 density after the CG atom of the Lys263 side chain (Figure S4C), this conserved lysine could provide
 258 another ligand for binding the extra heme.

259

260 Discussion

261 Leveraging a combination of sequence similarity clustering, phylogenetics, domain analysis, and
 262 identification of conserved gene neighbors, this study has provided a more complete understanding of the
 263 functional diversification among members of the split-barrel superfamily, broadly, and among plant and
 264 algae, specifically. Functional divergence has resulted in a wide-array of possible heme-utilization proteins
 265 in prokaryotes and distinct families of heme-degrading proteins and heme sensors in plants and algae,
 266 combined with additional subfamilies (many unique to land plants and/or algae) of unknown function.
 267 Using similarity to the SUPERFAMILY hidden Markov model SSF50475 (27) (Figure S1), which aligns
 268 to both the split-barrel domain and DRI region, we identified multiple separate protein subfamilies in
 269 analyzed land plant genomes (Figure 1). Three of these contain uncharacterized proteins (named “unknown-
 270 1” (e.g., AT3G49140, AT3G59300, and AT5G24060), “unknown-2” (e.g., AT3G04020), and “HOZ2”
 271 (e.g., AT1G51560 and AT3G21140)), while five subfamilies contain previously characterized proteins:
 272 PNPO (e.g., At5g49970/PDX3 (13, 28)), PNPO2 (e.g., AT2G46580 (29)), CREG (e.g., CREG from
 273 animals (14)), GBP (e.g., AT3G21200 (15, 16, 30–32)), and HOZ (named HOZ1; e.g., AT3G03890 (8))
 274 (Figure 1). Chlorophyte algal genomes encode members of these previously characterized subfamilies plus
 275 FLVA/FLVB (e.g., Cre12.g531900 and Cre16.g691800 (33)) and five subfamilies of uncharacterized
 276 proteins (unknown-2, HOZ2, unknown-3 (Cre07.g327079), unknown-4 (Cre03.g155350), and unknown-5
 277 (Cre06.g297600)) (Figure 1). The plant and green algal PNPO subfamily is distinguished by the presence
 278 of an N-terminal YjeF-like domain (defined by IPR004443), which encodes an epimerase involved in repair
 279 of NAD (13) (Figure 2A). The YjeF-like domain is not present in PNPO2 homologs (Figure 2A). Like
 280 PNPO2, CREG is also a single-domain protein (Figure 2A). CREG has not been characterized in plants and
 281 is related to the Cellular Repressor of E1A-stimulated Genes (*i.e.*, CREG), a secreted glycoprotein in
 282 animals, which interacts with the cation-independent mannose 6-phosphate/insulin-like growth factor II
 283 receptor to inhibit cellular proliferation (34). The other eight *A. thaliana* proteins all contain the heme-
 284 binding domain, DRI (22) (previously named DUF2470; defined by IPR037119) that is found in the heme-
 285 degradation proteins HugZ, ChuZ, and MSMEG_6519 (Figure 2A-E). Three of these DRI-containing
 286 proteins (AT3G49140, AT3G59300, and AT5G24060) match the SSF50475 model for belonging to the
 287 split-barrel superfamily (Figure S1) but do not match the split-barrel domain defined by IPR012349 (Figure
 288 2A). However, the split-barrel domain is evident in the computationally predicted structures with large
 289 unstructured loops inserted in the domain (Figure S2). The other *A. thaliana* homologs, including the
 290 previously characterized heme-sensor GBP (15, 32) and heme-degradation protein HOZ (8), all contain the
 291 split-barrel domain followed by DRI (Figure 2A), which is evident from the sequence and structure analysis
 292 (Figure 2A and 2C).

293

294 The closely related GBP, HOZ1, and HOZ2 subfamilies likely existed in the last common ancestor of
 295 Viridiplantae because of the presence of conserved Chlorophyte and Streptophyte orthologs in each
 296 subfamily (Figure 2F). They may have also already existed in the last common ancestor of Archeplastida,
 297 since we identified close homologs of HOZ1 and GBP in the glaucophyte alga *Cyanophora paradoxa* and
 298 red algae (Figure 2F). HOZ2, however, appears to be specific to Viridiplantae and was not identified in the
 299 available genomes of either red algae or protist algae that have chloroplasts derived from secondary
 300 endosymbiotic events (Figure 2F). Whether because of a horizontal gene transfer event or because a HOZ-
 301 like protein was present in a more ancient eukaryotic ancestor, we also identified HOZ-like proteins in some
 302 fungal genomes, but IPR037119/DRI was consistently not detected in these fungal proteins (Figure 2F).
 303 IPR037119/DRI is often not detected among orthologous eukaryotic split-barrel proteins, and this absence
 304 could be a result of sequence divergence (and therefore have poor similarity scores to IPR037119/DRI),

305 since some of these proteins tend to be as large or larger than the *A. thaliana* two-domain proteins (Figure
306 2F).

307
308 Our analysis also reveals a large number of uncharacterized HOZ-like proteins in prokaryotes. The
309 previously characterized HugZ-like and HutZ-like proteins represent only a small part of the larger heme-
310 binding split-barrel family (Figure 2) that includes uncharacterized proteins from *Pseudomonas aeruginosa*
311 (PA4388) and *Cupriavidus metallidurans* (Rmet_5353). Based on sequence similarity, domain architecture,
312 and conserved gene neighbors putatively involved in heme/iron assimilation (Figure 3), the prokaryotic
313 HOZ homologs are likely also involved in heme utilization like the HugZ proteins. Intriguingly, structural
314 diversification has resulted in three distinct heme-utilization subtypes within the heme-binding split-barrel
315 family: small single-domain HutZ-like (split-barrel domain only), two domain HugZ-like (DRI followed
316 by split-barrel domain), and two domain HOZ-like (split-barrel domain followed by DRI). Based on our
317 phylogenetic analysis of the split-barrel domain, the plant/algal HOZ family and bacterial HOZ-like
318 proteins, such as the heme-degradation protein MSMEG_6519 from *Mycobacterium smegmatis* (12),
319 represent an ancestral protein conformation: the split-barrel domain followed by DRI. The presence of
320 HOZ-like and HutZ-like proteins at the base of the HutZ-HugZ clade (Figure 2F, dashed line box) suggest
321 that HutZ evolved via loss of DRI, and HugZ subsequently evolved via an independent “re-fusion” event
322 involving the split-barrel domain with DRI added to the N-terminus. Combined with experimental
323 characterization of Dri1 from cyanobacteria, which contains DRI but lacks the split-barrel domain, DRI is
324 likely a regulatory domain and is not required for enzymatic function. Coincidentally, in Actinomycetota,
325 a group of canonical heme oxygenases containing DRI have also evolved (22), suggesting that the
326 regulatory function provided by DRI may be portable across convergently evolved heme-degrading
327 enzymes.

328
329 In addition to the three structural subtypes, published studies suggest that a small number of amino acid
330 changes can alter substrate preference and/or function. There are single-domain HutZ-like proteins that,
331 like HutZ, contain a C-terminal loop containing a conserved histidine residue important for heme *b*
332 degradation, whereas in Pden_1323 the C-terminal loop is missing, and the protein degrades heme *c* (19).
333 HupZ from *S. pyogenes* is also missing the histidine-containing loop but is hypothesized to be a heme
334 chaperone (20). For the two-domain HOZ-like proteins, there are homologs that degrade heme *b* (*i.e.*, HOZ1
335 (8)) and paralogs that have lost that ability and function as heme sensors (*i.e.*, GBP). Further diversification
336 can and has occurred with respect to subcellular location, as we experimentally verified for two closely
337 related HOZ1 paralogs in the tree *P. trichocarpa*. Gene duplication followed by a change in localization of
338 the encoded protein is a common adaptive mechanism (35–37). The duplication leading to the evolution of
339 the cytosolic HOZ1 likely occurred in the *Saliceae* ancestor, because of the presence of orthologs in *Salix*
340 and *Populus* species but absence in other *Salicaceae* members, suggesting a relatively recent (~48 million
341 years ago (38)) neofunctionalization event. The cytosolic paralog, PtHOZ1B, has retained *in vitro* heme-
342 degradation activity, but the *in vivo* function and the reason for maintaining this cytosolic protein in these
343 trees has yet to be determined.

344
345 Like AtHOZ1 and HugZ, PtHOZ1B forms a homodimer where the interaction interface involves the split-
346 barrel domain. There is very little difference between the previously determined crystal structure of the
347 AtHOZ1 dimer and the PtHOZ1B structure presented here (Figure S4A). The most striking distinction
348 between the two structures (other than the presence/absence of heme) is the metal-bound sites found in the
349 split-barrel domain of PtHOZ1B and in the DRI region. The imidazole of His90 in PtHOZ1B is rotated
350 roughly 100° compared to the corresponding residue (His135) in the AtHOZ1 structure where it interacts
351 with the propionic side chains of heme. One hypothesis is that this metal site is a regulatory site, and when
352 a metal ion is bound, His90 is prevented from binding the propionic side chains of heme. However, we
353 found that mutation of any one of the amino acid residues in metal site 1 inhibited the ability of PtHOZ1B
354 to rescue the yeast *hmx1Δ* strain, which does not support a role of this site in inhibiting heme degradation.
355 Although we cannot rule out the possibility that these mutations lead to misfolding or other unintended

356 impacts on activity, it seems likely that metal site 1 may represent a crystallization artifact. Metal site 2,
357 composed of two histidine residues that are almost absolutely conserved across DRI regions in homologous
358 proteins (22), may also be a heme-binding, rather than metal ion binding, site based on comparison to the
359 “extra” heme site of ChuZ. However, additional experimental work is needed to understand the occupancy
360 of these sites *in plantae* and how they relate to function.

361
362 Focusing on the plastid-localized HOZ subfamilies that are unique to plants and algae, we further
363 determined that these proteins likely play an important role in chloroplast physiology. *AtHOZ1* and
364 *AtHOZ2A* can both rescue the H₂O₂ sensitivity of the yeast *hmx1Δ* mutant, while mutation in *A. thaliana*
365 leads to significant developmental delays. These results are in contrast to the paralog *AtHOZ2B* that cannot
366 rescue the H₂O₂ sensitivity of the yeast *hmx1Δ* mutant, and the T-DNA line did not have any observable
367 growth defects under the conditions tested. Why loss of *AtHOZ1* and *AtHOZ2A* impacts growth is presently
368 unknown, especially as multiple plastid-localized heme oxygenases have been described in *A. thaliana* (39).
369 *In vitro*, *AtHOZ1* produces biliverdin and therefore could contribute to retrograde signaling and bilin
370 biosynthesis like the canonical heme oxygenases (8). If this is the case *in vivo*, then there may be
371 specialization in terms of gene/protein regulation and/or their protein-interaction networks compared to
372 other heme oxygenases.

373
374 Although inconclusive, we do note that compared to the land plant proteins, the *C. reinhardtii* *HOZ1*
375 ortholog exhibited relatively poor *in vitro* heme-binding and -degradation activity under the conditions
376 tested, and the gene failed to rescue the H₂O₂-sensitivity of the yeast *hmx1Δ* strain, in contrast to the *HOZ1*
377 genes from *A. thaliana*, *P. trichocarpa*, and *S. bicolor*. Therefore, further work is needed to determine
378 whether the molecular function of the *C. reinhardtii* protein has diverged compared to the land plant
379 orthologs or the protein performed poorly in these assays (due to mis-folding or some other issue). Although
380 we were unable to provide conclusive evidence as to whether *C. reinhardtii* *HOZ1* has heme-degradation
381 activity, we did observe that, like in *A. thaliana*, loss of *HOZ1* impacts growth when a reduced carbon
382 source is not available, pointing to a physiological function related to the chloroplast. These results suggest
383 an ancient function of the *HOZ1* family tied to the evolution of photosynthesis in eukaryotes. The recent
384 identification of a suppressor mutation in *C. reinhardtii*, which compensates for loss of the canonical heme
385 oxidase *HMOX1*, supports the existence of an alternative bilin biosynthetic pathway (40). Although the
386 genetic mutation responsible for the published phenotype rescue was not determined, a mutation, such as
387 disruption of a repressor, that leads to constitutive expression of *CrHOZ1* (if *CrHOZ1* functions in heme-
388 degradation) is one hypothesis.

389
390 Out of the eight DRI-containing proteins in *A. thaliana*, only those encoded by *AtHOZ1* and *AtHOZ2A*
391 were able to complement the loss of the heme oxidase gene in *S. cerevisiae* (Figure 4B). This implies that
392 in addition to *HOZ1*, *HOZ2* proteins can potentially degrade heme, whereas other homologs, such as *GBP*,
393 may have lost enzymatic activity and could function as regulators. However, there are many other viable
394 reasons why these genes did not complement the *hmx1Δ* mutation, and further biochemical studies would
395 be needed to rule out *in vitro* heme-degradation activity. In the case of *GBP*, the inability to rescue the H₂O₂
396 sensitivity is expected, since this homolog is a relatively well-characterized heme sensor and regulator of
397 tetrapyrrole biosynthesis (15, 31). Intriguingly, the evolution of non-enzymatic family members has
398 happened in the canonical heme oxygenase family as well; proteins belonging to the HO-1 subfamily are
399 able to bind and degrade heme, while HO-2 subfamily members are unable to do so, but rather bind to the
400 precursor protoporphyrin IX (41). Like *GBP*, the function of the HO-2 subfamily has been hypothesized to
401 be involved in the regulation of tetrapyrrole biosynthesis. Therefore, in parallel to the canonical heme
402 oxygenase family, the presence of multiple HOZ-like protein families in plants and algae might serve to
403 fine tune tetrapyrrole metabolism: preventing heme-induced toxicity, facilitating iron salvaging, and
404 regulating the production of heme, chlorophyll, and intermediates. Nonetheless, whereas the expansion of
405 the canonical heme oxygenase family is specific to land plants, *HOZ1* and *HOZ2* represent two distinct
406 families that were already present in the last common ancestor shared between chlorophytes and

407 streptophytes. As such, there may also be some biochemical differences that underly distinct biological
 408 roles in the chloroplast, which have been conserved during evolution of Viridiplantae. However, at this
 409 point, other than complementation of the *hmx1Δ* mutation in yeast by *AtHOZ2A* and a growth defect in *A.*
 410 *thaliana*, very little is known about this HOZ-like family.

411
 412

413 **Experimental procedures**

414
 415

415 **Bioinformatic analyses**

416 All sequence similarity networks were constructed using the EFI-EST tool (<http://efi.igb.illinois.edu/efi-est/>) (42) and visualized with Cytoscape v3.9.1 using the Prefuse Force Directed Layout incorporating the
 417 alignment scores. The FMN-binding split-barrel superfamily sequence similarity network (in Figure 1) was
 418 constructed by searching the UniProt (43), Phytozome (44) and PhycoCosm databases (45) for the split-
 419 barrel family defined by a match to SSF50475. An alignment score of 20 was used to build the network,
 420 and the nodes were collapsed based on a sequence identity of 90%. Node information is available in Table
 421 S2. To construct the HOZ family sequence similarity network (in Figure 3A), the split-barrel family
 422 members identified with SSF50475 from *A. thaliana*, which contain the DRI region (IPR037119), were
 423 used to search against UniProt using BLASTp. The network was constructed using an alignment score of
 424 20; sequences were trimmed to the domain boundaries set by IPR037119; nodes were collapsed based on
 425 95% identity. Node information is available in Table S3. Domain cartoons were drawn based on domain
 426 predictions in InterPro (46). TargetP was used to predict transit peptides (47). Gene neighborhoods were
 427 collected and visualized using the EFI-GNT webtool (42); predicted protein names were based on searches
 428 of NCBI Conserved Domain Database. The following structural models were used for visualizing 3D
 429 domains and were downloaded from the AlphaFold protein structure database (AF;
 430 <https://alphafold.ebi.ac.uk/>) or from the Protein Data Bank (PDB; <https://www.rcsb.org/>) (48): GBP, PDB:
 431 5YJL (49); HOZ1, PDB: 6M0A; PNPO1, AF: Q9LTX3; PNPO2, AF: Q9ZPY1; HOZ2A, AF: Q8VXY3;
 432 HOZ2B, AF: Q8L637; AT3G49140, AF: Q0WMN5; AT3G59300, AF: Q949V7; AT5G24060, AF:
 433 F4KFP8; CREG, AF: Q8RY62; HutZ, PDB: 3TGV; HugZ, PDB: 3GAS; MSMEG_6519, PDB: 5BNC
 434 (12); Dri1, PDB: 8GDW (22). When required, unstructured N-terminal sequence was removed for better
 435 visualization. For the tree containing proteins similar to the HOZ family (in Figure 2F), subsequences
 436 representing IPR012349 were collected and aligned with MAFFT (50) and then used to construct a
 437 phylogenetic tree using FastTREE (51) with default parameters on CIPRES Science Gateway (52);
 438 *AtPNPO1/PDX3* was used as an outgroup. Annotation information for each leaf (taxonomy, domain and
 439 domain order, and protein length) was downloaded from UniProt. For the plant HOZ tree (in Figure 4A),
 440 the phylogenetic tree was constructed using IQ-TREE webserver (53) with an alignment from COBALT
 441 (54) that was manually edited to remove sequences flanking the split-barrel and DRI regions. Trees were
 442 annotated and visualized with iTOL (55). For both trees, branches with a score less than 50% for bootstrap
 443 support were deleted. Sequence information, multiple sequence alignments and Newick trees can be found
 444 in Tables S4 and S5.

445
 446

447 **Localization**

448 The subcellular localizations of proteins of interest were tested in poplar leaf mesophyll protoplasts as
 449 previously described (56). The cDNAs of Potri.013G057700, Potri.019G035200, and Sobic.002G349100
 450 were synthesized and cloned into the pTwist ENTR Kozak plasmid using the clonal gene service of Twist
 451 Bioscience and then subcloned into the transient expression vector pUC-pGWB505 via LR reaction
 452 (Invitrogen) for C-terminal YFP fusion (56). Three transient expression plasmids were used to express
 453 organelle markers: PM-mCherry is the plasmid membrane marker constructed by cloning the expression
 454 cassette of CD3-1007 (57) plasmid into pUC19, plastid-mCherry is the plastid marker constructed by
 455 cloning the expression cassette of CD3-1000 (57) plasmid into pUC19, the nuclear marker nucleus-
 456 mCherry is the mCherry-VirD2NLS plasmid (58). The pUC-pGWB505 construct (8 μg) was co-transfected
 457 with 2 μg of corresponding organelle marker plasmid into 100 μl of protoplasts (~2 x 10⁴ cells) to determine

458 their subcellular localizations. After 16 h incubation under weak light at room temperature, protoplasts were
459 collected and resuspended in cold W5 solution (2 mM MES pH 5.7, 154 mM NaCl, 125 mM CaCl₂, and 5
460 mM KCl) to subject to microscopy. Images were collected using a Leica TCS SP5 confocal microscope,
461 equipped with 514 and 543 nm laser lines for excitation of YFP and mCherry, respectively. The emission
462 bandwidth for YFP and mCherry was 500-530 nm and 580-620 nm, respectively. Images were processed
463 using LAS X software (Leica).

464

465 **Protein expression and purification**

466 The *E. coli*-codon-optimized synthetic CDS (Twist Bioscience) of Potri.013G057700, Potri.019G035200,
467 and Sobic.002G349100 were cloned into the *Nde*I and *Xho*I sites of the pET29b vector carrying C-terminal
468 TEV cleavage site followed by 6 × His-Tag sequence. The Cre02.g098250 gene construct was designed
469 and assembled by the Joint Genome Institute (JGI) and cloned into the pET11e vector (22). The coding
470 sequences of the N-terminal transit peptides were not included in the DNA synthesis. The plasmids
471 encoding the plant HOZs were transformed into competent *E. coli* BL21(DE3) cells. Multiple colonies from
472 the transformed plate were picked and incubated in LB medium containing 100 µg/ml kanamycin overnight
473 at 37 °C. The cells were inoculated into 500 ml of auto-induction ZYM-50521 medium and grown at 37 °C
474 to an OD₆₀₀ of about 0.6. The cells were then allowed to auto-induce overnight at 20 °C (59). The cells
475 were harvested by centrifugation at 5,000 rpm for 20 min, lysed at ice-cold temperature using bacterial
476 protein extraction agent (B-PER, Thermo Fisher Scientific) in the presence of 300mM NaCl, 30mM Tris
477 pH 8.0, lysozyme and benzonase. The soluble and insoluble fractions were separated by centrifugation at
478 18,000 rpm for 20 min. The resulting cell-free supernatant was allowed to bind for 20 min at 20 °C with
479 Ni-NTA agarose (Thermo scientific) resin that had earlier been equilibrated with buffer A (40 mM Tris,
480 400 mM NaCl, 5% glycerol, 10 mM imidazole, pH 8.0). This mixture was then poured into a column and
481 the resin was washed with a 50 ml buffer A. The protein was eluted using a step gradient with increasing
482 concentration of imidazole (50, 100 and 250 mM). Fractions of the eluate were analyzed on 4–10% SDS–
483 PAGE gel. The histidine tag was cleaved by TEV protease followed by reverse nickel-affinity
484 chromatography. Further purification was achieved with a size-exclusion column (Superdex increase-200)
485 that had previously been equilibrated with buffer that consisted of 40 mM HEPES, 2 mM TCEP, 3%
486 glycerol, 150 mM NaCl, pH 7.0. Purified proteins were concentrated to ~12 mg/mL and stored at -80 °C.
487 The selenomethionine of PtHOZ1B was expressed in a BASM SeMet medium and purified in the same
488 way as native.

489

490 **Heme-binding and degradation assays**

491 Heme-binding assays were conducted following the protocol from Leung *et al.* (60). Briefly, a
492 concentration of 5 µM of purified proteins from *P. trichocarpa* (Potri.013G057700, Potri.019G035200), *S.*
493 *bicolor* (Sobic.002G349100) and *C. reinhardtii* (Cre02.g098250) were used for titration in 850 µL of buffer
494 (50 mM HEPES, 200 mM NaCl, pH 7.5). Fresh hemin stock solutions were prepared by dissolving hemin
495 with a few drops of 0.1 M NaOH, and 1 mL ultrapure water. Following filtration through a 0.22 µm filter,
496 the hemin concentration was quantified at 385 nm ($\epsilon_{385\text{ nm}} = 58.4\text{ mM}^{-1}\text{ cm}^{-1}$). Spectra were recorded in
497 quartz cuvettes (pathlength 1 mm) using a NanoDrop One^c Spectrophotometer (Thermo Scientific). Heme
498 titration was performed by incrementally adding hemin (from 0 µM to 14.8 µM) to the protein, incubating
499 for 3 minutes, and collecting the spectra. The formation of a characteristic Soret peak (~405 nm) indicates
500 heme binding. Heme degradation was assayed by monitoring the UV-Vis absorption spectra kinetics of the
501 protein (5 µM) in the presence of hemin (5 µM) and ascorbate (10 mM) as electron donor in 50 mM HEPES,
502 200 mM NaCl, pH 7.5. Kinetics were started by addition of ascorbate (t₀) and monitored every 3 min for
503 170 min.

504

505 **Crystallization, data collection and structure determination of PtHOZ1B**

506 The SeMet PtHOZ1B crystals were grown at 20 °C by the sitting drop vapor diffusion method, using a 1:1
507 ratio of protein: reservoir solution containing 20% PEG monomethyl ether 2000, 10 mM nickel chloride
508 and 100 mM sodium acetate pH 5.0. Before data collection, crystals were transferred into mother liquor

509 containing 20% glycerol and then flash cooled in liquid nitrogen. The X-ray diffraction data were collected
 510 at the FMX (17-ID-2) beamline of NSLS-II, Brookhaven National Laboratory (BNL), Upton, NY, United
 511 States. Crystals of PtHOZ1B were diffracted to 1.8 Å resolution and the data were processed with
 512 HKL20002 (61). The Matthews coefficient (VM) was calculated as 2.2 Å³ Da⁻¹, which corresponds to one
 513 molecule per asymmetric unit with an estimated solvent content of 45%. The structure of PtHOZ1B was
 514 determined by SAD technique with SAD phasing pipeline of PHASER in the CCP4 program suite (62, 63).
 515 The structure was refined by several rounds of iterative model building with COOT5 and refinement in
 516 CCP4 module, REFMAC (64, 65). A summary of the data-collection and refinement statistics are shown
 517 in Table S1. The final model contains one PtHOZ1B molecule, two nickel ions, and 97 waters. The N-
 518 terminal 20 amino acids were not included in the model due to lack of electron density. Also, the regions
 519 Ala144 to Phe149 and Val168 to Gly174 were disordered and exhibited poor electron density. The model
 520 was evaluated and deposited in the PDB (PDB id: 9BL1). ChimeraX-1.8 was used to visualize and align
 521 structures (66).

522

523 **Plant Materials**

524 *A. thaliana* Columbia-0 (Col-0) seeds were surface sterilized with 20% bleach and dH₂O. T-DNA insertion
 525 lines SALK_025420C for HOZ2A (AT1G51560) and SALK_001793 for HOZ2B (AT3G21140) were
 526 obtained from the ABRC stock center (Figure S3). Primers GCCAGAAGAGCAGCAAGTGAG and
 527 TGCATGGTGTCTCTTCATCA were used to verify T-DNA insertion in *HOZ2A*. Primers
 528 GAAGGATGGGCTGAAAACGAC and TTACTIONCCCCGAGCTTTTCCTTCAC were used to verify T-
 529 DNA insertion in *HOZ2B*. The seeds were stratified in darkness at 4°C for three days. The greenhouse was
 530 maintained at 22°C with a light density of ~100 μmol m⁻²s⁻¹ with 16 hr light / 8 hr dark cycle.

531

532 **CRISPR-Cas9 mutagenesis of *HOZ1***

533 Two guide RNAs (ACATCTAGGAACATAATCTAG and TGAGAGGAGAAAATCGACGG) mapping to
 534 the first exon of *AtHOZ1* were designed and checked for off-targets using the website CRISPR-P
 535 <http://crispr.hzau.edu.cn/CRISPR2/> (67). CRISPR-Cas9 plasmids were generated according to the protocol
 536 and materials outlined in the Golden Gate Molecular Cloning Kit (68). The sgRNAs were amplified using
 537 pICH86966::AtU6p::sgRNA_PDS (AddGene) as a template. Level 1 guides were assembled with
 538 pICH47751-NOSpro:NPTII and pICH47742-35Spro:Cas9 into binary level 2 vector pAGM4723. The final
 539 binary vectors were transformed into *A. thaliana* Col-0 by *Agrobacterium tumefaciens* (GV3101), using
 540 floral dipping methods outlined by (69). T1 and T2 plants were selected by red fluorescence, *i.e.*, seeds
 541 with red seed coat color would be used for T1, and Cas9-free T2 plants would be seeds with no red seed
 542 coat (70). To increase the efficiency of mutagenesis, 10-day-old T1 plants were treated with cycles of 30
 543 hours at 37°C, and 42 hours at 22°C (71). To identify the homozygous gene-edited lines, a 0.5 mm leave
 544 disc from each plant was used as a template for PCR using KAPA 3G Plant PCR Kit (Roche) with primers
 545 flanking the edited region (*HOZCR* forward primer: CTGCATCCCTCTCCTCCAAC, *HOZCR* reverse
 546 primer: CACTGTTGCCACTCCCGTAAG). PCR products were analyzed by sanger sequencing by both
 547 sequences and chromatograms (Figure S3). Identical procedures were carried out for two generations of
 548 plants. T3 plants with gene sequences that match wild-type *HOZ1* were used as the WT control, and
 549 independent deletions that caused a frame-shift or stop-gain were analyzed. The triple *AtHOZ2A AtHOZ2B*
 550 *AtHOZ1* mutant was generated as outlined above, except that the *hoz2a hoz2b* mutant (generated by
 551 crossing SALK_025420C and SALK_001793) was used to transform the CRISPR-Cas9 construct. The
 552 sequenced mutation of the *hoz1* allele is identical to *hoz1-7*.

553

554 **Yeast complementation assay**

555 Yeast *hmx1* and plant HOZ coding sequences were PCR amplified and cloned into a yeast expression vector
 556 for the yeast complementation assay (Table S6). The yeast gene *hmx1* was amplified from genomic DNA
 557 of *S. cerevisiae* BY4742. All *A. thaliana* genes were PCR amplified from whole plant cDNA. *S. bicolor*,
 558 *P. trichocarpa* and *C. reinhardtii* genes were PCR amplified from the synthetic genes synthesized from
 559 Twist Bioscience, also used for heterologous protein purification. Site-directed mutagenesis on PtHOZ1B

560 was achieved using the megaprimers method (primers in Table S6). The PCR-amplified genes were cloned
 561 into *XmaI/EcoRI* digested P413-GPD plasmid using Gibson assembly. The p413-GPD plasmids containing
 562 the different genes and empty p413-GPD were transformed by lithium acetate method into *hmx1Δ* strain
 563 (from the Yeast matalpha collection; Horizon Discovery), and empty p413-GPD also transformed into WT
 564 strain BY4742. Complementation assay was performed by growing yeast cells in SD-His until saturation.
 565 Five microliters of ten-fold serial dilutions (10^0 , 10^{-1} , 10^{-2}) were spotted on agar solidified YPD with or
 566 without 3 mM H₂O₂. Plates were incubated at 30 °C and imaged at 3 days post inoculation.

567

568 **Chlamydomonas growth**

569 Three independent *C. reinhardtii* cell lines mutated for *CrHOZ1* (Cre02.g098250), LMJ.RY0402.068342,
 570 LMJ.RY0402.099542, LMJ.RY0402.105224, and the WT strain LMJ.RY0402 were obtained from the
 571 Chlamydomonas Library Project (CLiP) (72). Chlamydomonas cells were pre-cultured in liquid TAP media
 572 at 24 °C and shaken at 250 rpm in an Innova[®] 44/44R shaker (New Brunswick) for 5 days with a light
 573 intensity of 100 μmol m⁻² s⁻¹ photons. Cells were washed twice with TP media, and inoculated in TP or
 574 TAP media containing different concentrations of Fe (0.1 μM, 1μM, 20 μM and 75 μM) as indicated, at an
 575 OD_{750nm} of 0.05 and grown for 6 days in 24-well plates in triplicates (n=3).

576

577 **Data availability**

578 All data supporting this study are reported within this manuscript and/or supplemental files. Raw data are
 579 available from the corresponding author upon reasonable request. Atomic coordinates and structure factors
 580 for the PtHOZ1 structure were deposited into the Protein Data Bank as 9BL1. Requests for resources and
 581 reagents generated in this study are available from the Lead Contact with a completed Materials Transfer
 582 Agreement.

583

584 **Supporting information**

585 This article contains supporting information.

586

587 **Funding and additional information**

588 This work was supported by the U.S. Department of Energy, Office of Science, Office of Biological and
 589 Environmental Research, as part of the Quantitative Plant Science Initiative at Brookhaven National
 590 Laboratory. Work at the Molecular Foundry was supported by the Office of Science, Office of Basic Energy
 591 Sciences, of the U.S. Department of Energy under Contract No. DE-AC02-05CH11231. The work (Award
 592 DOI <https://doi.org/10.46936/10.25585/60000750>) conducted by the U.S. Department of Energy Joint
 593 Genome Institute (<https://ror.org/04xm1d337>), a DOE Office of Science User Facility, is supported by the
 594 Office of Science of the U.S. Department of Energy operated under Contract No. DE-AC02-05CH11231.
 595 The work at Cold Spring Harbor Laboratory was supported by U.S. Department of Agriculture, Agricultural
 596 Research Service awards 8062-21000-051-000D.

597

598 **Conflict of interest**

599 The authors declare that they have no conflicts of interest with the contents of this article.

600

601 **References**

- 602 1. Kumar, S., and Bandyopadhyay, U. (2005) Free heme toxicity and its detoxification
 603 systems in human. *Toxicol Lett.* 10.1016/j.toxlet.2005.03.004
- 604 2. Chiabrando, D., Vinchi, F., Fiorito, V., Mercurio, S., and Tolosano, E. (2014) Heme in
 605 pathophysiology: A matter of scavenging, metabolism and trafficking across cell
 606 membranes. *Front Pharmacol.* 10.3389/fphar.2014.00061
- 607 3. Hirotsu, S., Chu, G. C., Unno, M., Lee, D. S., Yoshida, T., Park, S. Y., Shiro, Y., and Ikeda-
 608 Saito, M. (2004) The Crystal Structures of the Ferric and Ferrous Forms of the Heme

- 609 Complex of HmuO, a Heme Oxygenase of *Corynebacterium diphtheriae*. *Journal of*
610 *Biological Chemistry*. **279**, 11937–11947
- 611 4. Schuller, D. J., Wilks, A., Ortiz De Montellano, P. R., and Poulos, T. L. (1999) Crystal
612 structure of human heme oxygenase-1. *Nat Struct Biol*. 10.1038/12319
- 613 5. Haley, K. P., Janson, E. M., Heilbronner, S., Foster, T. J., and Skaar, E. P. (2011)
614 *Staphylococcus lugdunensis* IsdG liberates iron from host heme. *J Bacteriol*. **193**, 4749–
615 4757
- 616 6. Wu, R., Skaar, E. P., Zhang, R., Joachimiak, G., Gornicki, P., Schneewind, O., and
617 Joachimiak, A. (2005) *Staphylococcus aureus* IsdG and IsdI, heme-degrading enzymes
618 with structural similarity to monooxygenases. *Journal of Biological Chemistry*.
619 10.1074/jbc.M409526200
- 620 7. Lojek, L. J., Farrand, A. J., Wisecaver, J. H., Blaby-Haas, C. E., Michel, B. W., Merchant, S.
621 S., Rokas, A., and Skaar, E. P. (2017) *Chlamydomonas reinhardtii* LFO1 Is an IsdG Family
622 Heme Oxygenase. *mSphere*. **2**, e00176-17
- 623 8. Wang, J., Guo, Q., Li, X., Wang, X., and Liu, L. (2020) The Arabidopsis locus AT3G03890
624 encodes a dimeric β -barrel protein implicated in heme degradation. *Biochemical Journal*.
625 10.1042/BCJ20200712
- 626 9. Liu, X., Gong, J., Wei, T., Wang, Z., Du, Q., Zhu, D., Huang, Y., Xu, S., and Gu, L. (2012)
627 Crystal structure of HutZ, a heme storage protein from *Vibrio cholerae*: A structural
628 mismatch observed in the region of high sequence conservation. *BMC Struct Biol*.
629 10.1186/1472-6807-12-23
- 630 10. Hu, Y., Jiang, F., Guo, Y., Shen, X., Zhang, Y., Zhang, R., Guo, G., Mao, X., Zou, Q., and
631 Wang, D. C. (2011) Crystal structure of HugZ, a novel heme oxygenase from *Helicobacter*
632 *pylori*. *Journal of Biological Chemistry*. 10.1074/jbc.M110.172007
- 633 11. Kitamura, M., Kojima, S., Ogasawara, K., Nakaya, T., Sagara, T., Niki, K., Miura, K. I.,
634 Akutsu, H., and Kumagai, I. (1994) Novel FMN-binding protein from *Desulfovibrio vulgaris*
635 (Miyazaki F). Cloning and expression of its gene in *Escherichia coli*. *Journal of Biological*
636 *Chemistry*. 10.1016/s0021-9258(17)37499-9
- 637 12. Ahmed, F. H., Carr, P. D., Lee, B. M., Afriat-Jurnou, L., Mohamed, A. E., Hong, N. S.,
638 Flanagan, J., Taylor, M. C., Greening, C., and Jackson, C. J. (2015) Sequence-Structure-
639 Function Classification of a Catalytically Diverse Oxidoreductase Superfamily in
640 Mycobacteria. *J Mol Biol*. **427**, 3554–3571
- 641 13. Colinas, M., Shaw, H. V., Loubéry, S., Kaufmann, M., Moulin, M., and Fitzpatrick, T. B.
642 (2014) A pathway for repair of NAD(P)H in plants. *Journal of Biological Chemistry*.
643 10.1074/jbc.M114.556092
- 644 14. Ghobrial, G., Araujo, L., Jinwala, F., Li, S., and Lee, L. Y. (2018) The structure and biological
645 function of CREG. *Front Cell Dev Biol*. 10.3389/fcell.2018.00136
- 646 15. Czarnecki, O., Hedtke, B., Melzer, M., Rothbart, M., Richter, A., Schröter, Y.,
647 Pfannschmidt, T., and Grimm, B. (2011) An Arabidopsis GluTR binding protein mediates
648 spatial separation of 5-Aminolevulinic acid synthesis in chloroplasts. *Plant Cell*.
649 10.1105/tpc.111.086421
- 650 16. Sinha, N., Eirich, J., Finkemeier, I., and Grimm, B. (2022) Glutamate 1-semialdehyde
651 aminotransferase is connected to GluTR by GluTR-binding protein and contributes to the
652 rate-limiting step of 5-aminolevulinic acid synthesis. *Plant Cell*. **34**, 4623–4640

- 653 17. Guo, Y., Guo, G., Mao, X., Zhang, W., Xiao, J., Tong, W., Liu, T., Xiao, B., Liu, X., Feng, Y.,
654 and Zou, Q. (2008) Functional identification of HugZ, a heme oxygenase from
655 *Helicobacter pylori*. *BMC Microbiol.* **8**, 226
- 656 18. Uchida, T., Sekine, Y., Matsui, T., Ikeda-Saito, M., and Ishimori, K. (2012) A heme
657 degradation enzyme, HutZ, from *Vibrio cholerae*. *Chemical Communications*.
658 10.1039/c2cc31147j
- 659 19. Li, S., Isiorho, E. A., Owens, V. L., Donnan, P. H., Odili, C. L., and Mansoorabadi, S. O.
660 (2021) A noncanonical heme oxygenase specific for the degradation of c-type heme.
661 *Journal of Biological Chemistry*. 10.1016/j.jbc.2021.100666
- 662 20. Lyles, K. V., Thomas, L. S., Ouellette, C., Cook, L. C. C., and Eichenbaum, Z. (2022) HupZ, a
663 Unique Heme-Binding Protein, Enhances Group A *Streptococcus* Fitness During Mucosal
664 Colonization. *Front Cell Infect Microbiol.* 10.3389/fcimb.2022.867963
- 665 21. Zhang, R., Zhang, J., Guo, G., Mao, X., Tong, W., Zhang, Y., Wang, D. C., Hu, Y., and Zou, Q.
666 (2011) Crystal structure of *Campylobacter jejuni* ChuZ: a split-barrel family heme
667 oxygenase with a novel heme-binding mode. *Biochem. Biophys. Res. Commun.* **415**, 82–87
- 668 22. Grosjean, N., Yee, E. F., Kumaran, D., Chopra, K., Abernathy, M., Biswas, S., Byrnes, J.,
669 Kreitler, D. F., Cheng, J.-F., Ghosh, A., Almo, S. C., Iwai, M., Niyogi, K. K., Pakrasi, H. B.,
670 Sarangi, R., van Dam, H., Yang, L., Blaby, I. K., and Blaby-Haas, C. E. (2024) A hemoprotein
671 with a zinc-mirror heme site ties heme availability to carbon metabolism in
672 cyanobacteria. *Nat Commun.* **15**, 3167
- 673 23. Gerdes, S., El Yacoubi, B., Bailly, M., Blaby, I. K., Blaby-Haas, C. E., Jeanguenin, L., Lara-
674 Núñez, A., Pribat, A., Waller, J. C., Wilke, A., Overbeek, R., Hanson, A. D., and de Crécy-
675 Lagard, V. (2011) Synergistic use of plant-prokaryote comparative genomics for
676 functional annotations. *BMC Genomics*. 10.1186/1471-2164-12-S1-S2
- 677 24. Collinson, E. J., Wimmer-Kleikamp, S., Gerega, S. K., Yang, Y. H., Parish, C. R., Dawes, I.
678 W., and Stocker, R. (2011) The yeast homolog of heme oxygenase-1 affords cellular
679 antioxidant protection via the transcriptional regulation of known antioxidant genes.
680 *Journal of Biological Chemistry*. 10.1074/jbc.M110.187062
- 681 25. Lin, Q., Weis, S., Yang, G., Weng, Y. H., Helston, R., Rish, K., Smith, A., Bordner, J., Polte,
682 T., Gaunitz, F., and Dennerly, P. A. (2007) Heme oxygenase-1 protein localizes to the
683 nucleus and activates transcription factors important in oxidative stress. *Journal of*
684 *Biological Chemistry*. 10.1074/jbc.M607954200
- 685 26. Krause, K., Oetke, S., and Krupinska, K. (2012) Dual targeting and retrograde
686 translocation: Regulators of plant nuclear gene expression can be sequestered by
687 plastids. *Int J Mol Sci.* 10.3390/ijms130911085
- 688 27. Gough, J., Karplus, K., Hughey, R., and Chothia, C. (2001) Assignment of homology to
689 genome sequences using a library of hidden Markov models that represent all proteins of
690 known structure. *J Mol Biol.* 10.1006/jmbi.2001.5080
- 691 28. Sang, Y., Barbosa, J. M., Wu, H., Locy, R. D., and Singh, N. K. (2007) Identification of a
692 pyridoxine (pyridoxamine) 5'-phosphate oxidase from *Arabidopsis thaliana*. *FEBS Lett.*
693 10.1016/j.febslet.2006.12.028
- 694 29. Sang, Y., Goertzen, L. R., Tzou, Y. M., Locy, R. D., and Singh, N. K. (2011) Identification of a
695 second pyridoxine (pyridoxamine) 5'-phosphate oxidase in *Arabidopsis thaliana*. *Acta*
696 *Physiol Plant.* 10.1007/s11738-010-0579-6

- 697 30. Jung, H. S., Okegawa, Y., Shih, P. M., Kellogg, E., Abdel-Ghany, S. E., Pilon, M., Sjolander,
698 K., Shikanai, T., and Niyogi, K. K. (2010) Arabidopsis thaliana PGR7 encodes a conserved
699 chloroplast protein that is necessary for efficient photosynthetic electron transport. *PLoS*
700 *One*. 10.1371/journal.pone.0011688
- 701 31. Apitz, J., Nishimura, K., Schmied, J., Wolf, A., Hedtke, B., van Wijk, K. J., and Grimm, B.
702 (2016) Posttranslational Control of ALA Synthesis Includes GluTR Degradation by Clp
703 Protease and Stabilization by GluTR-Binding Protein. *Plant Physiol.* **170**, 2040–2051
- 704 32. Richter, A. S., Banse, C., and Grimm, B. (2019) The GluTR-binding protein is the heme-
705 binding factor for feedback control of glutamyl-tRNA reductase. *Elife*.
706 10.7554/eLife.46300
- 707 33. Chaux, F., Burlacot, A., Mekhalfi, M., Auroy, P., Blangy, S., Richaud, P., and Peltier, G.
708 (2017) Flavodiiron proteins promote fast and transient O₂ photoreduction in
709 chlamydomonas. *Plant Physiol.* 10.1104/pp.17.00421
- 710 34. Di Bacco, A., and Gill, G. (2003) The secreted glycoprotein CREG inhibits cell growth
711 dependent on the mannose-6-phosphate/insulin-like growth factor II receptor.
712 *Oncogene*. 10.1038/sj.onc.1206670
- 713 35. Panchy, N., Lehti-Shiu, M., and Shiu, S. H. (2016) Evolution of gene duplication in plants.
714 *Plant Physiol.* 10.1104/pp.16.00523
- 715 36. Liu, S. L., Pan, A. Q., and Adams, K. L. (2014) Protein subcellular relocation of
716 duplicated genes in Arabidopsis. *Genome Biol Evol.* 10.1093/gbe/evu191
- 717 37. Marques, A. C., Vinckenbosch, N., Brawand, D., and Kaessmann, H. (2008) Functional
718 diversification of duplicate genes through subcellular adaptation of encoded proteins.
719 *Genome Biol.* 10.1186/gb-2008-9-3-r54
- 720 38. Bell, C. D., Soltis, D. E., and Soltis, P. S. (2010) The age and diversification of the
721 angiosperms re-revisited. *Am J Bot.* 10.3732/ajb.0900346
- 722 39. Emborg, T. J., Walker, J. M., Noh, B., and Vierstra, R. D. (2006) Multiple heme oxygenase
723 family members contribute to the biosynthesis of the phytochrome chromophore in
724 arabidopsis. *Plant Physiol.* **140**, 856–868
- 725 40. Zhang, W., Deng, R., Shi, W., Li, Z., Larkin, R. M., Fan, Q., and Duanmu, D. (2022) Heme
726 oxygenase-independent bilin biosynthesis revealed by a hmx1 suppressor screening in
727 Chlamydomonas reinhardtii. *Front Microbiol.* 10.3389/fmicb.2022.956554
- 728 41. Gisk, B., Yasui, Y., Kohchi, T., and Frankenberg-Dinkel, N. (2010) Characterization of the
729 haem oxygenase protein family in Arabidopsis thaliana reveals a diversity of functions.
730 *Biochemical Journal.* 10.1042/BJ20090775
- 731 42. Zallot, R., Oberg, N., and Gerlt, J. A. (2019) The EFI Web Resource for Genomic
732 Enzymology Tools: Leveraging Protein, Genome, and Metagenome Databases to Discover
733 Novel Enzymes and Metabolic Pathways. *Biochemistry.* 10.1021/acs.biochem.9b00735
- 734 43. Bateman, A., Martin, M. J., Orchard, S., Magrane, M., Agivetova, R., Ahmad, S., Alpi, E.,
735 Bowler-Barnett, E. H., Britto, R., Bursteinas, B., Bye-A-Jee, H., Coetzee, R., Cukura, A.,
736 Silva, A. Da, Denny, P., Dogan, T., Ebenezer, T. G., Fan, J., Castro, L. G., Garmiri, P.,
737 Georghiou, G., Gonzales, L., Hatton-Ellis, E., Hussein, A., Ignatchenko, A., Insana, G.,
738 Ishtiaq, R., Jokinen, P., Joshi, V., Jyothi, D., Lock, A., Lopez, R., Luciani, A., Luo, J., Lussi, Y.,
739 MacDougall, A., Madeira, F., Mahmoudy, M., Menchi, M., Mishra, A., Moulang, K.,
740 Nightingale, A., Oliveira, C. S., Pundir, S., Qi, G., Raj, S., Rice, D., Lopez, M. R., Saidi, R.,

- 741 Sampson, J., Sawford, T., Speretta, E., Turner, E., Tyagi, N., Vasudev, P., Volynkin, V.,
 742 Warner, K., Watkins, X., Zaru, R., Zellner, H., Bridge, A., Poux, S., Redaschi, N., Aimo, L.,
 743 Argoud-Puy, G., Auchincloss, A., Axelsen, K., Bansal, P., Baratin, D., Blatter, M. C.,
 744 Bolleman, J., Boutet, E., Breuza, L., Casals-Casas, C., de Castro, E., Echioukh, K. C.,
 745 Coudert, E., Cuche, B., Doche, M., Dornevil, D., Estreicher, A., Famiglietti, M. L.,
 746 Feuermann, M., Gasteiger, E., Gehant, S., Gerritsen, V., Gos, A., Gruaz-Gumowski, N.,
 747 Hinz, U., Hulo, C., Hyka-Nouspikel, N., Jungo, F., Keller, G., Kerhornou, A., Lara, V., Le
 748 Mercier, P., Lieberherr, D., Lombardot, T., Martin, X., Masson, P., Morgat, A., Neto, T. B.,
 749 Paesano, S., Pedruzzi, I., Pilbout, S., Pourcel, L., Pozzato, M., Pruess, M., Rivoire, C.,
 750 Sigrist, C., Sonesson, K., Stutz, A., Sundaram, S., Tognolli, M., Verbregue, L., Wu, C. H.,
 751 Arighi, C. N., Arminski, L., Chen, C., Chen, Y., Garavelli, J. S., Huang, H., Laiho, K.,
 752 McGarvey, P., Natale, D. A., Ross, K., Vinayaka, C. R., Wang, Q., Wang, Y., Yeh, L. S., and
 753 Zhang, J. (2021) UniProt: The universal protein knowledgebase in 2021. *Nucleic Acids Res.*
 754 10.1093/nar/gkaa1100
- 755 44. Goodstein, D. M., Shu, S., Howson, R., Neupane, R., Hayes, R. D., Fazo, J., Mitros, T.,
 756 Dirks, W., Hellsten, U., Putnam, N., and Rokhsar, D. S. (2012) Phytozome: A comparative
 757 platform for green plant genomics. *Nucleic Acids Res.* 10.1093/nar/gkr944
- 758 45. Grigoriev, I. V., Hayes, R. D., Calhoun, S., Kamel, B., Wang, A., Ahrendt, S., Dusheyko, S.,
 759 Nikitin, R., Mondo, S. J., Salamov, A., and others (2021) PhycoCosm, a comparative algal
 760 genomics resource. *Nucleic Acids Res.* **49**, D1004--D1011
- 761 46. Blum, M., Chang, H. Y., Chuguransky, S., Grego, T., Kandasaamy, S., Mitchell, A., Nuka, G.,
 762 Paysan-Lafosse, T., Qureshi, M., Raj, S., Richardson, L., Salazar, G. A., Williams, L., Bork,
 763 P., Bridge, A., Gough, J., Haft, D. H., Letunic, I., Marchler-Bauer, A., Mi, H., Natale, D. A.,
 764 Necci, M., Orengo, C. A., Pandurangan, A. P., Rivoire, C., Sigrist, C. J. A., Sillitoe, I., Thanki,
 765 N., Thomas, P. D., Tosatto, S. C. E., Wu, C. H., Bateman, A., and Finn, R. D. (2021) The
 766 InterPro protein families and domains database: 20 years on. *Nucleic Acids Res.*
 767 10.1093/nar/gkaa977
- 768 47. Armenteros, J. J. A., Salvatore, M., Emanuelsson, O., Winther, O., Von Heijne, G.,
 769 Elofsson, A., and Nielsen, H. (2019) Detecting sequence signals in targeting peptides
 770 using deep learning. *Life Sci Alliance.* 10.26508/lsa.201900429
- 771 48. Berman, H. M., Westbrook, J., Feng, Z., Gilliland, G., Bhat, T. N., Weissig, H., Shindyalov, I.
 772 N., and Bourne, P. E. (2000) The Protein Data Bank. *Nucleic Acids Res.*
 773 10.1093/nar/28.1.235
- 774 49. Zhao, A., and Han, F. (2018) Crystal structure of Arabidopsis thaliana glutamyl-tRNA_{Glu}
 775 reductase in complex with NADPH and glutamyl-tRNA_{Glu} reductase binding protein.
 776 *Photosynth Res.* 10.1007/s11120-018-0518-8
- 777 50. Katoh, K., and Standley, D. M. (2013) MAFFT multiple sequence alignment software
 778 version 7: improvements in performance and usability. *Mol Biol Evol.* **30**, 772–780
- 779 51. Price, M. N., Dehal, P. S., and Arkin, A. P. (2010) FastTree 2 - Approximately maximum-
 780 likelihood trees for large alignments. *PLoS One.* **5**, e9490
- 781 52. Miller, M., Pfeiffer, W., and Schwartz, T. (2010) Creating the CIPRES science gateway for
 782 inference of large phylogenetic trees, p 11572--8. in *Proceedings of the Gateway*
 783 *Computing Environments Workshop (GCE). Institute of Electrical and Electronics*
 784 *Engineers, Piscataway, NJ. [http://dx. doi. org/10.1109/GCE](http://dx.doi.org/10.1109/GCE)*

- 785 53. Trifinopoulos, J., Nguyen, L. T., von Haeseler, A., and Minh, B. Q. (2016) W-IQ-TREE: a fast
786 online phylogenetic tool for maximum likelihood analysis. *Nucleic Acids Res.* **44**, W232–
787 W235
- 788 54. Papadopoulos, J. S., and Agarwala, R. (2007) COBALT: Constraint-based alignment tool
789 for multiple protein sequences. *Bioinformatics.* **23**, 1073–1079
- 790 55. Letunic, I., and Bork, P. (2021) Interactive tree of life (iTOL) v5: An online tool for
791 phylogenetic tree display and annotation. *Nucleic Acids Res.* 10.1093/nar/gkab301
- 792 56. Xie, M., Muchero, W., Bryan, A. C., Yee, K., Guo, H. B., Zhang, J., Tschaplinski, T. J., Singan,
793 V. R., Lindquist, E., Payyavula, R. S., Barros-Rios, J., Dixon, R., Engle, N., Sykes, R. W.,
794 Davis, M., Jawdy, S. S., Gunter, L. E., Thompson, O., Difazio, S. P., Evans, L. M., Winkeler,
795 K., Collins, C., Schmutz, J., Guo, H., Kalluri, U., Rodriguez, M., Feng, K., Chen, J. G., and
796 Tuskan, G. A. (2018) A 5-enolpyruvylshikimate 3-phosphate synthase functions as a
797 transcriptional repressor in populus. *Plant Cell.* **30**, 1645–1660
- 798 57. Nelson, B. K., Cai, X., and Nebenführ, A. (2007) A multicolored set of in vivo organelle
799 markers for co-localization studies in Arabidopsis and other plants. *Plant Journal.*
800 10.1111/j.1365-313X.2007.03212.x
- 801 58. Lee, L. Y., Fang, M. J., Kuang, L. Y., and Gelvin, S. B. (2008) Vectors for multi-color
802 bimolecular fluorescence complementation to investigate protein-protein interactions in
803 living plant cells. *Plant Methods.* 10.1186/1746-4811-4-24
- 804 59. Studier, F. W. (2005) Protein production by auto-induction in high density shaking
805 cultures. *Protein Expr Purif.* 10.1016/j.pep.2005.01.016
- 806 60. Leung, G. C. H., Fung, S. S. P., Dovey, N. R. B., Raven, E. L., and Hudson, A. J. (2019)
807 Precise determination of heme binding affinity in proteins. *Anal Biochem.*
808 10.1016/j.ab.2019.02.021
- 809 61. Otwinowski, Z., and Minor, W. (1997) Processing of X-ray diffraction data collected in
810 oscillation mode. *Methods Enzymol.* 10.1016/S0076-6879(97)76066-X
- 811 62. Winn, M. D., Ballard, C. C., Cowtan, K. D., Dodson, E. J., Emsley, P., Evans, P. R., Keegan,
812 R. M., Krissinel, E. B., Leslie, A. G. W., McCoy, A., McNicholas, S. J., Murshudov, G. N.,
813 Pannu, N. S., Potterton, E. A., Powell, H. R., Read, R. J., Vagin, A., and Wilson, K. S. (2011)
814 Overview of the CCP4 suite and current developments. *Acta Crystallogr D Biol*
815 *Crystallogr.* 10.1107/S0907444910045749
- 816 63. McCoy, A. J., Grosse-Kunstleve, R. W., Adams, P. D., Winn, M. D., Storoni, L. C., and Read,
817 R. J. (2007) Phaser crystallographic software. *J Appl Crystallogr.*
818 10.1107/S0021889807021206
- 819 64. Emsley, P., and Cowtan, K. (2004) Coot: Model-building tools for molecular graphics. *Acta*
820 *Crystallogr D Biol Crystallogr.* 10.1107/S0907444904019158
- 821 65. Murshudov, G. N., Vagin, A. A., and Dodson, E. J. (1997) Refinement of macromolecular
822 structures by the maximum-likelihood method. *Acta Crystallogr D Biol Crystallogr.*
823 10.1107/S0907444996012255
- 824 66. Goddard, T. D., Huang, C. C., Meng, E. C., Pettersen, E. F., Couch, G. S., Morris, J. H., and
825 Ferrin, T. E. (2018) UCSF ChimeraX: Meeting modern challenges in visualization and
826 analysis. *Protein Science.* **27**, 14–25

- 827 67. Lei, Y., Lu, L., Liu, H. Y., Li, S., Xing, F., and Chen, L. L. (2014) CRISPR-P: A web tool for
 828 synthetic single-guide RNA design of CRISPR-system in plants. *Mol Plant*.
 829 10.1093/mp/ssu044
- 830 68. Engler, C., Youles, M., Gruetzner, R., Ehnert, T. M., Werner, S., Jones, J. D. G., Patron, N.
 831 J., and Marillonnet, S. (2014) A Golden Gate modular cloning toolbox for plants. *ACS*
 832 *Synth Biol*. 10.1021/sb4001504
- 833 69. Clough, S. J., and Bent, A. F. (1998) Floral dip: A simplified method for *Agrobacterium*-
 834 mediated transformation of *Arabidopsis thaliana*. *Plant Journal*. **16**, 735–743
- 835 70. Gao, X., Chen, J., Dai, X., Zhang, D., and Zhao, Y. (2016) An effective strategy for reliably
 836 isolating heritable and Cas9-free *Arabidopsis* mutants generated by CRISPR/Cas9-
 837 mediated genome editing. *Plant Physiol*. **171**, 1794–1800
- 838 71. LeBlanc, C., Zhang, F., Mendez, J., Lozano, Y., Chatpar, K., Irish, V. F., and Jacob, Y. (2018)
 839 Increased efficiency of targeted mutagenesis by CRISPR/Cas9 in plants using heat stress.
 840 *Plant Journal*. 10.1111/tpj.13782
- 841 72. Li, X., Patena, W., Fauser, F., Jinkerson, R. E., Saroussi, S., Meyer, M. T., Ivanova, N.,
 842 Robertson, J. M., Yue, R., Zhang, R., Vilarrasa-Blasi, J., Wittkopp, T. M., Ramundo, S.,
 843 Blum, S. R., Goh, A., Laudon, M., Srikumar, T., Lefebvre, P. A., Grossman, A. R., and
 844 Jonikas, M. C. (2019) A genome-wide algal mutant library and functional screen identifies
 845 genes required for eukaryotic photosynthesis. *Nat Genet*. 10.1038/s41588-019-0370-6
 846
 847

848 Figure legends

849
 850 **Figure 1** The split-barrel superfamily contains functionally distinct plant proteins. A sequence similarity
 851 network is shown of proteins from *Arabidopsis thaliana* (At) and *Chlamydomonas reinhardtii* (Cr) that
 852 belong to the split-barrel superfamily (defined as inclusion in SSF50475) and their homologs. Nodes are
 853 colored by taxonomy according to the color key. Clusters are named based on members with characterized
 854 or predicted function. Clusters with *A. thaliana* and/or *C. reinhardtii* homologs of unknown function are
 855 labeled unknown “1” through unknown “5”. Pink background shading is used to highlight separate clusters,
 856 and dotted red lines are used to delineate subclusters. A grey box is used to indicate those clusters containing
 857 proteins that are a fusion between the split-barrel domain and DRI. The location of nodes representing *A.*
 858 *thaliana* and *C. reinhardtii* proteins are indicated with a white arrow and label, as is the CREG protein from
 859 *Homo sapiens*. Abbreviations and locus IDs for protein names: DRI: domain related to iron, PNPO:
 860 pyridoxine 5'-phosphate oxidase, CREG: cellular repressor of E1A-stimulated genes, FLV: flavodiiron,
 861 HOZ: homolog of HugZ, GBP: GluTR-binding protein, AtPPOX2: AT2G46580, AtGBP: AT3G21200,
 862 AtHOZ1: AT3G03890, AtHOZ2A: AT1G51560, AtHOZ2B: AT3G21140, AtPPOX: At5g49970,
 863 AtPPOX2: At2g46580, CrGTPBP1: Cre03.g156600, CrFLVB: Cre16.g691800, CrFLVA: Cre12.g531900,
 864 CrPPO1: Cre08.g378200, CrPNPO: Cre02.g095100, CrHOZ2: Cre12.g520200, CrHOZ1: Cre02.g098250.

865 **Figure 2** The split-barrel domain is found in a large family of prokaryotic and eukaryotic proteins linked
 866 to heme utilization. *A*, scaled cartoons of split-barrel superfamily members from *A. thaliana* depicting
 867 presence and location of transit peptides, the YjeF domain, the split-barrel domain (defined by IPR012349),
 868 and DRI. Locus IDs: AtPNPO1: At5g49970, AtPNPO2: AT2G46580, AtCREG: At2g04690, AtGBP:
 869 AT3G21200, AtHOZ1: AT3G03890, AtHOZ2A: AT1G51560, AtHOZ2B: AT3G21140. Numbers in
 870 parentheses refer to the numbered clusters in Fig. 1. *B*, scaled cartoons depicting representative bacterial
 871 proteins related to the eukaryotic HOZ family. *C*, experimental (PDB ID given) or computationally
 872 predicted structural models for *A. thaliana* proteins containing IPR012349. Corresponding pLDDT
 873 confidence measures for the computationally predicted structures can be found in Figure S1. *D*,

874 computationally predicted structural models of *A. thaliana* proteins from cluster unknown “1”.
 875 Corresponding pLDDT confidence measures for the computationally predicted structures can be found in
 876 Figure S1. *E*, experimentally determined structural models of bacterial proteins that serve as representatives
 877 for the 4 common types of identified domain architectures. For panels *A-E*, the split-barrel domain is colored
 878 orange, the YjeF domain is colored blue, and DRI is colored yellow. Stretches of sequences that do not
 879 match to an available domain model are colored grey. *F*, approximate maximum likelihood phylogenetic
 880 tree of the split-barrel domain sequences from the HOZ family and related homologs. Leaves representing
 881 *A. thaliana* proteins are labeled, as are proteins shown in panel *B*. Taxonomic information (T), domain
 882 architecture (D), and protein length (L) for each leaf is given at the bottom according to the color key.

883 **Figure 3** Prokaryotic homologs of the eukaryotic HOZ family are linked to Fe and heme utilization. *A*,
 884 protein sequence similarity network of HOZ-family proteins and homologs. Nodes are colored according
 885 to the color key. Nodes representing *Arabidopsis thaliana* (At) and *Chlamydomonas reinhardtii* (Cr) HOZ
 886 proteins are labelled, as are some uncharacterized proteins from well-studied bacteria. Pink background
 887 shading is used to highlight separate clusters, and dotted red lines are used to delineate subclusters. *B*,
 888 representative gene neighborhoods where genes encoding prokaryotic HOZ-like homologs are in close
 889 proximity to genes encoding proteins predicted to be involved in Fe assimilation based on presence of
 890 conserved domains (colored according to the color key). Genes encoding proteins that are not obviously
 891 related to Fe or heme utilization are grey. The number in parentheses is the UniProt ID for the HOZ-like
 892 protein. Protein name labels are derived from searches against NCBI’s Conserved Domain Database. *C*,
 893 representative proteins from each named prokaryotic cluster showing domain architecture.

894 **Figure 4** The HOZ family in plants may contain multiple heme-degradation proteins. *A*, maximum-
 895 likelihood phylogenetic tree of HOZ family proteins from Viridiplantae and selected bacteria. Tree leaves
 896 are colored according to the color key. Proteins from *Arabidopsis thaliana* (At), *Populus trichocarpa* (Pt),
 897 *Sorghum bicolor* (Sb), *Vitis vinifera* (Vv), *Zea mays* (Zm) and *Chlamydomonas reinhardtii* (Cr) are labeled,
 898 and the presence of a plastid transit peptide in these sequences is indicated with a green pentagon. Protein
 899 names in bold font were experimentally tested for heme-degradation in this study. Locus IDs starting with
 900 “Potri” are from *P. trichocarpa*, “VIT” are from *V. vinifera*, “Sobic” are from *S. bicolor*, and “Zm” are
 901 from *Z. mays*. *B*, yeast complementation to assess the functionality of *HOZ1* from *A. thaliana*, *P.*
 902 *trichocarpa*, *S. bicolor*, and *C. reinhardtii* and HOZ-like proteins from *A. thaliana*. *HOZ1* and HOZ-like
 903 proteins were overexpressed in the yeast mutant *hmx1Δ* lacking the canonical heme oxidase Hxm1p and
 904 assayed for their growth on YPD media in the absence or presence of 3 mM H₂O₂. AtGBP and AtCREG
 905 are used as negative controls. Original plate images can be found in Figure S6. From left to right, cultures
 906 were plated without diluting, diluting 10-fold or diluting 100-fold. The images were captured after 3 days
 907 at 30°C. Proteins names and corresponding locus IDs: AtHOZ1: AT3G03890, PtHOZ1B:
 908 Potri.013G057700, PtHOZ1A: Potri.019G035200, SbHOZ1: Sobic.002G349100, CrHOZ1:
 909 Cre02.g098250, AtHOZ2B: AT3G21140, AtHOZ2A: AT1G51560, AtGBP: AT3G21200, AtCREG:
 910 AT2G04690, VvHOZ1: VIT_208s0007g07350, ZmHOZ1: Zm00001d021881, CrHOZ2: Cre12.g520200,
 911 AtHOZ2B, VvHOZ2: VIT_209s0054g00600, PtHOZ2A: Potri.008G006400, PtHOZ2B:
 912 Potri.010G252300, ZmHOZ2A: Zm00001d031540, ZmHOZ2B: Zm00001d015274, ZmHOZ2C:
 913 Zm00001d037710, SbHOZ2A: Sobic.007G200700, SbHOZ2B: Sobic.007G200900, ZmHOZ2B:
 914 Zm00001d015274, ZmHOZ2C: Zm00001d015274, ZmHOZ2C: Zm00001d037710, SbHOZ2C:
 915 Sobic.004G040600, CrGTRBP1: Cre03.g156600, ZmGBPA: Zm00001d049343, ZmGBPB:
 916 Zm00001d021251, SbGBP: Sobic.007G090400

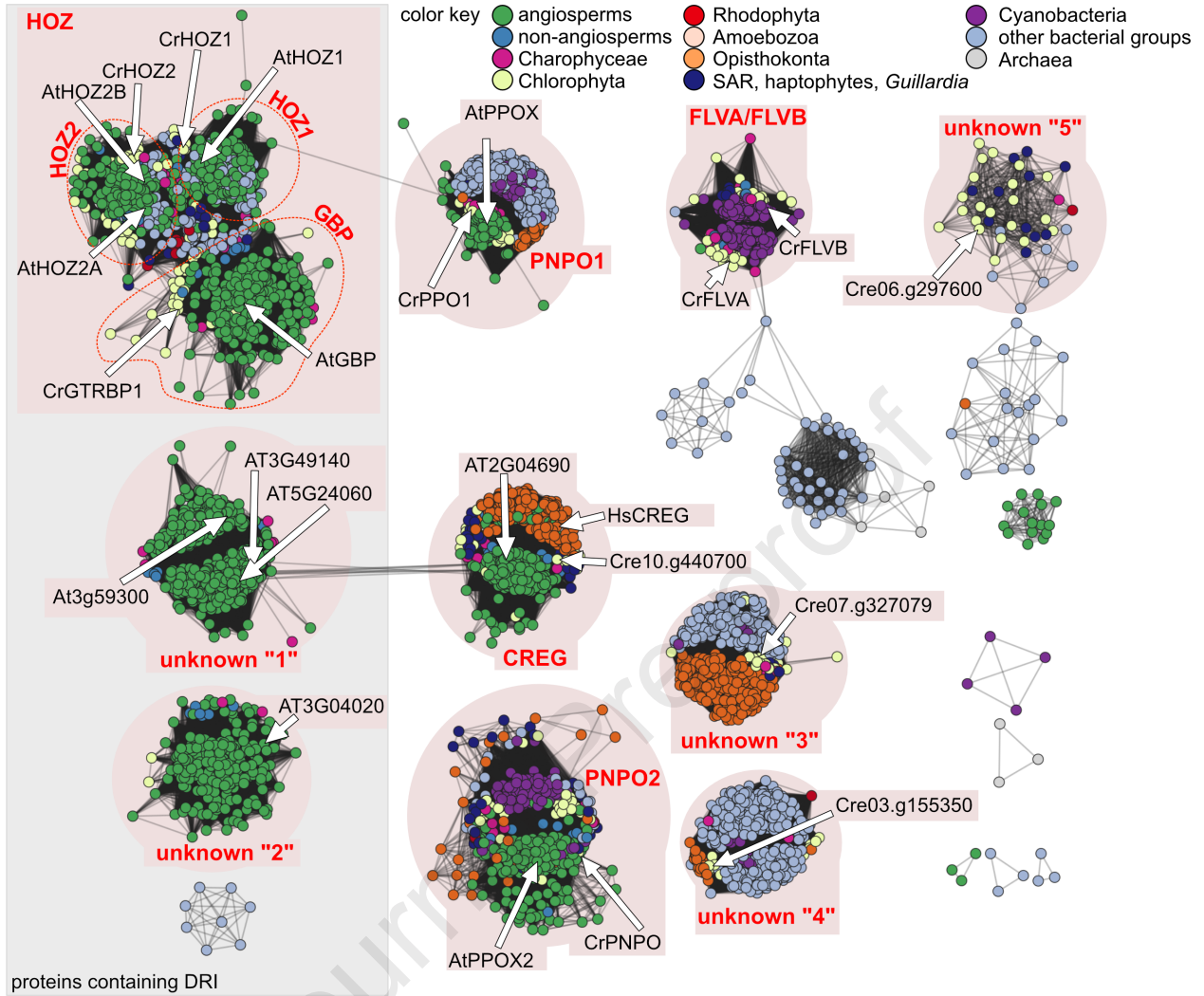
917 **Figure 5** The *in vitro* ability to degrade heme is conserved in the cytosolic *Populus trichocarpa* paralog.
 918 *A-C*, subcellular localization of HOZ1 homologs in *P. trichocarpa* (PtHOZ1B: Potri.013G057700 and
 919 PtHOZ1A: Potri.019G035200) and *Sorghum bicolor* (SbHOZ1: Sobic.002G349100). Proteins were fused
 920 with YFP at the C-terminus and transiently expressed in *P. trichocarpa* mesophyll protoplasts (green). The
 921 mCherry-fused organelle markers are co-expressed and shown in red. PM-mCherry, plasmid membrane

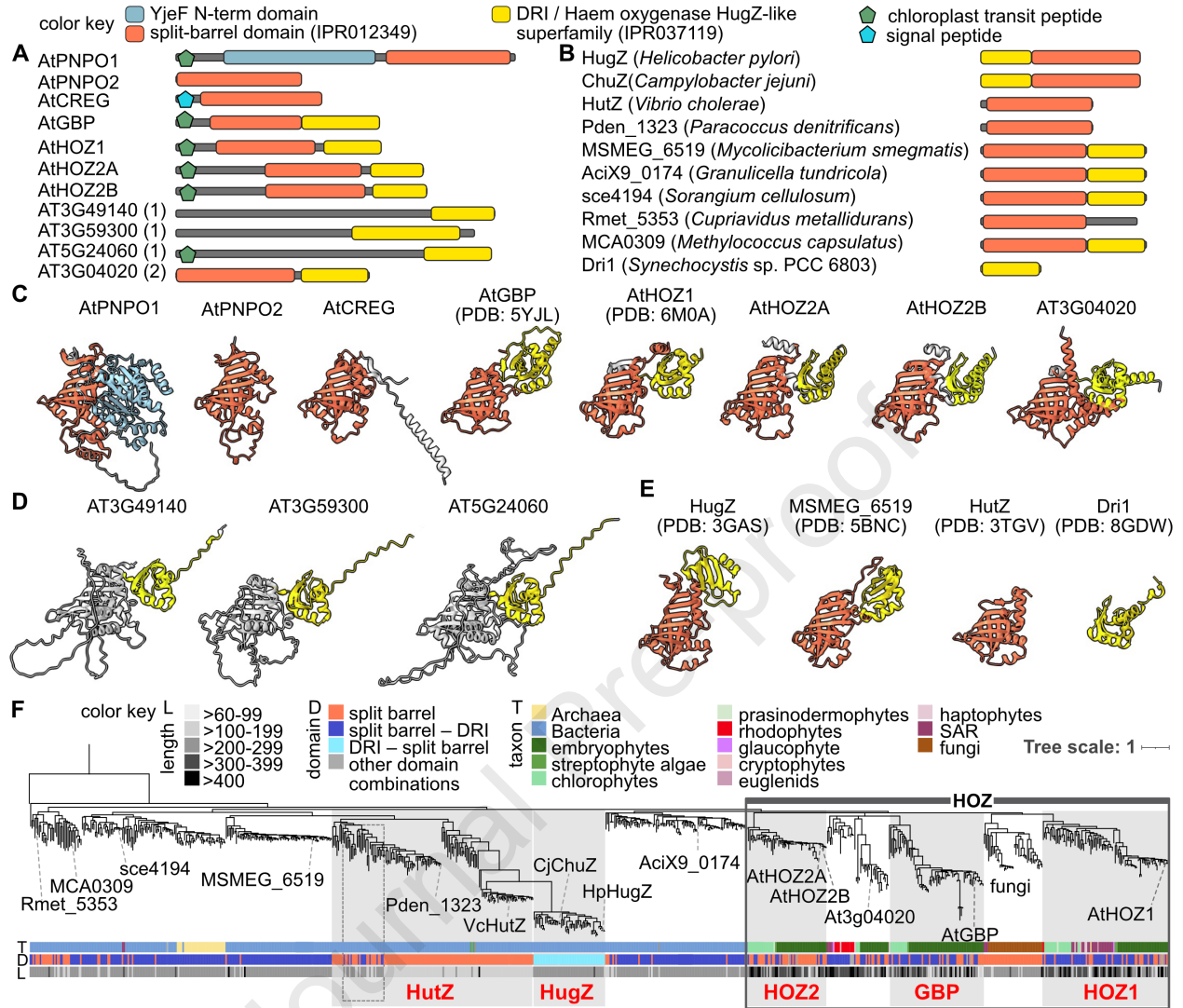
922 marker cloned from CD3-1007 plasmid; Plastid-mCherry, plastid marker cloned from CD3-1000 plasmid;
 923 Nucleus-mCherry, mCherry-VirD2NLS plasmid. Scale bar = 5 μm . *D*, UV-Vis absorption spectra of heme
 924 binding by *Chlamydomonas reinhardtii* (Cre02.g098250), *P. trichocarpa* and *S. bicolor* HOZ1 homologs
 925 showing a characteristic Soret peak at 405 nm indicating heme binding. Red spectra correspond to free
 926 hemin. Spectra gradient from light blue to dark blue correspond to the protein spectra with increasing heme
 927 concentration. *E* and *F*, UV-Vis absorption spectra kinetics of heme-bound HOZs in the absence (panel *E*)
 928 or presence (panel *F*) of ascorbate as the electron donor. Blue-colored spectrum represents $t = 0$ min, and
 929 red-colored spectrum represents $t = 170$ min. *G* and *H*, *C. reinhardtii* mutants and parental strain were
 930 grown in photo-heterotrophic (TAP) (panel *G*) or photo-autotrophic (TP) (panel *H*) conditions for 6 days
 931 with various concentrations of Fe, as indicated. *I*, growth curve of *C. reinhardtii* cells in Fe-replete TP
 932 media (20 μM Fe) for 6 days. For panels *G-I*, each circle represents the average of three separate biological
 933 replicates and the error bars represent the standard deviation. *Crhoz-1*, *Crhoz-2*, and *Crhoz*-refer to
 934 LMJ.RY0402.068342, LMJ.RY0402.099542, LMJ.RY0402.105224, respectively, three independent *C.*
 935 *reinhardtii* cell lines with mutations in *CrHOZ1*. The WT strain used is LMJ.RY0402.

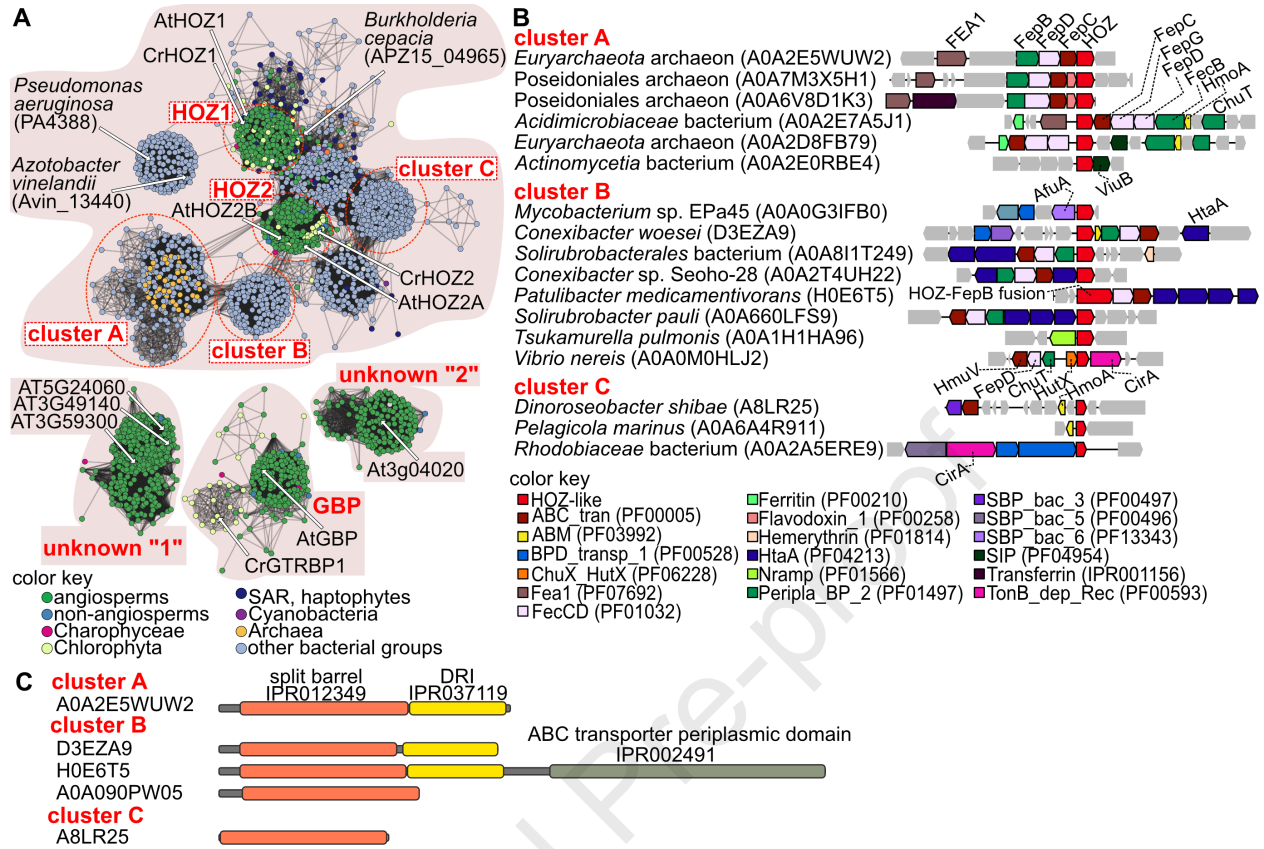
936 **Figure 6** Mutation of *AtHOZ1* and *AtHOZ2A* led to a developmental delay in *Arabidopsis thaliana*. Images
 937 of soil-potted plants were taken 28 days after sowing (DAS). A scale bar corresponding to the height of
 938 plants is given on the left. WT-1 refers to Col-1 wild-type plants, WT-2 refers to plants acquired after
 939 transformation of Col-0 with the CRISPR-Cas construct and are WT at the *AtHOZ1* gene, the *hoz1-1* and
 940 *hoz1-3* are independent mutants with different length deletions in the coding region of *AtHOZ1*, *hoz2a* and
 941 *hoz2b* refer to T-DNA lines of *AtHOZ2A* and *AtHOZ2B*, respectively, *hoz2a hoz2b* refer to the double
 942 mutant, and *hoz1-1 hoz2a hoz2b* is a triple mutant. Pictures of plants from 31, 34, 36, and 40 days after
 943 sowing are available in (Figure S7).

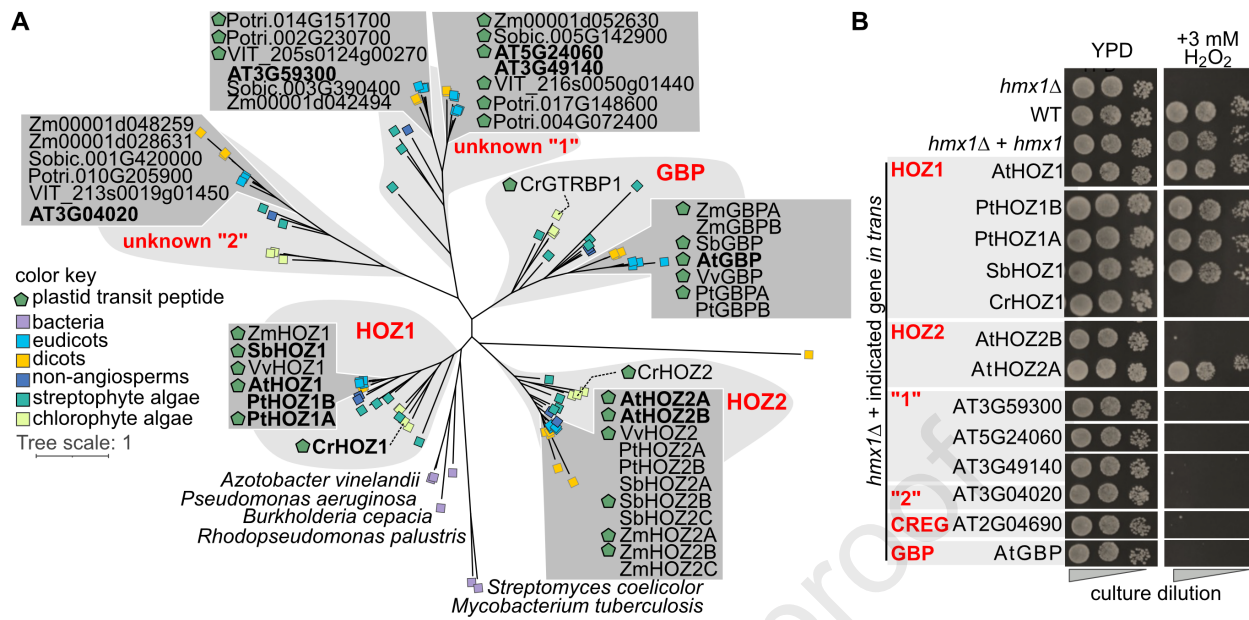
944 **Figure 7** The structure of cytosolic PtHOZ1B. *A*, ribbon cartoon of the observed PtHOZ1B homodimer.
 945 Chain A is colored light grey, and chain B is colored based on whether the corresponding sequence matches
 946 to the split-barrel domain (orange) or DRI (yellow). Dark grey indicates the amino acid residues
 947 corresponding to the linker that remains after cleavage of the His-tag. The two metal-sites are labelled. On
 948 the right, only chain B is shown and is rotated by 90°. *B*, alignment of the PtHOZ1B and AtHOZ1 (PDB:
 949 6M0A) structures using the matchmaker command implemented in ChimeraX-1.8. The root mean square
 950 deviation (RMSD) between 206 pruned atom pairs is 0.965 Å. Chains are colored according to the color
 951 key and the heme from AtHOZ1 is in red. *C*, alignment of the split-barrel domain dimers from PtHOZ1B,
 952 AtHOZ1 and HugZ (PDB: 3GAS) using the matchmaker command implemented in ChimeraX-1.8. For
 953 PtHOZ1B and HugZ, the root mean square deviation (RMSD) between 70 pruned atom pairs is 1.228 Å.
 954 The backbone and hemes are colored according to the key. A close-up view of the metal and heme sites,
 955 surrounded by a grey box, is given in panel *D*. *D*, close-up view of the metal and heme binding sites in the
 956 split-barrel domain dimer, highlighted with a box in panel *C*. The close-up is rotated relative to panel *C* to
 957 give a better view of the sites. *E*, alignment of PtHOZ1B with the DRI region of ChuZ (PDB: 3swj) using
 958 the matchmaker command implemented in ChimeraX-1.8. RMSD between 49 pruned atom pairs is 0.891
 959 Å. The “extra” heme found in the ChuZ structure is colored red. *F*, surface representation of PtHOZ1B with
 960 a heme modeled in the DRI region based on the alignment with ChuZ. *G*, close-up of metal site 2 that
 961 overlaps with the “extra” heme site of ChuZ. Top, surface representation of PtHOZ2A with metal-binding
 962 histidine residues of PtHOZ1B and heme-binding histidine residues of ChuZ shown as stick representations.
 963 A close-by asparagine in ChuZ that is in an equivalent position as an aspartic acid in PtHOZ1B is also
 964 shown as is the conserved lysine predicted to face toward the iron atom of the heme. The lysine in ChuZ is
 965 not modelled due to lack of electron density. Bottom, the same view, but the surface representation was
 966 removed to show alignment of the backbones. Throughout, “Pt” refers to *Populus trichocarpa*, “At” is
 967 *Arabidopsis thaliana*, and “Hp” is *Helicobacter pylori*.

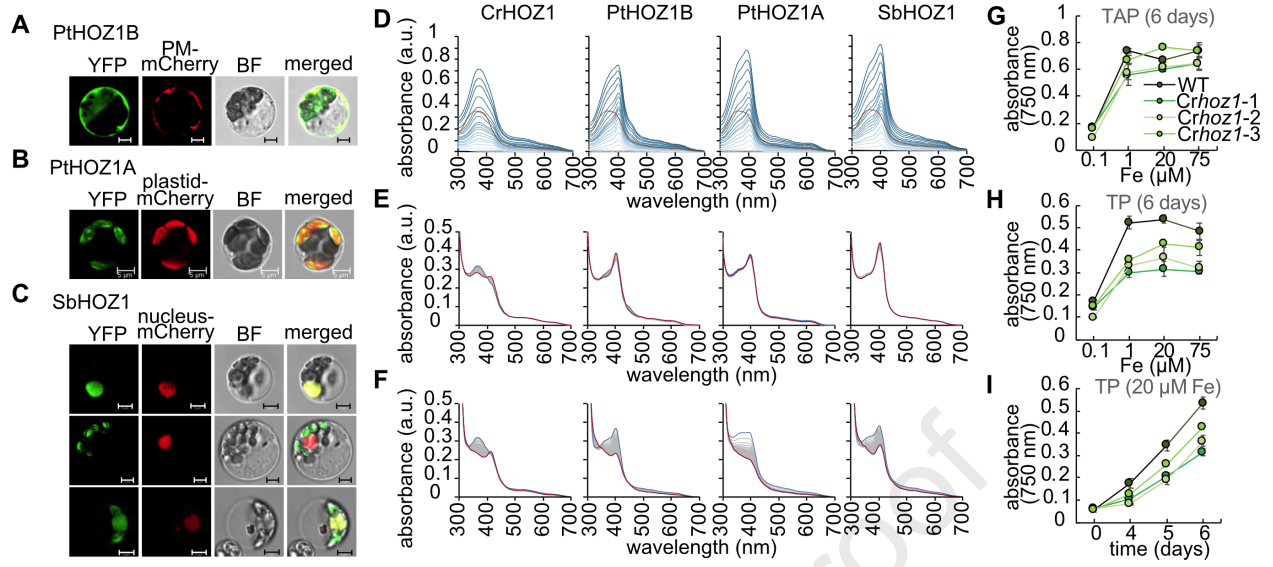
968
 969





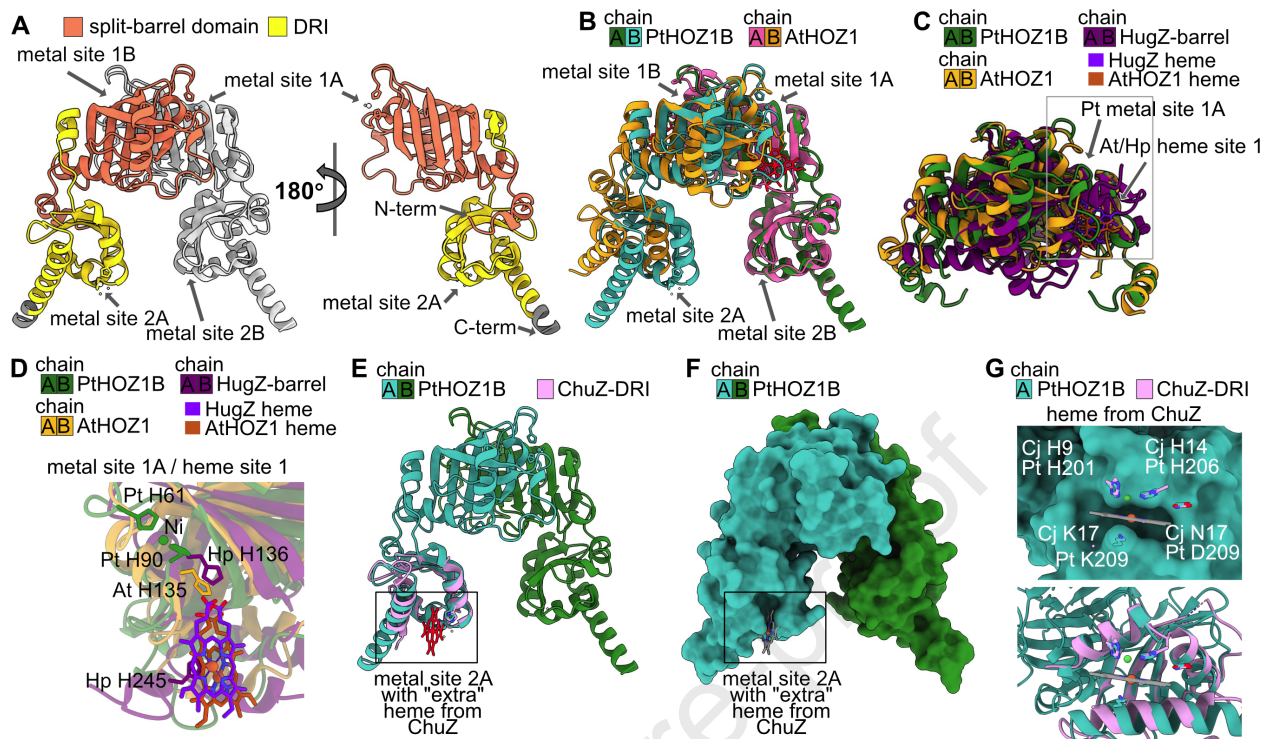








Journal Pre-proof



Declaration of interests

The authors declare that they have no known competing financial interests or personal relationships that could have appeared to influence the work reported in this paper.

The author is an Editorial Board Member/Editor-in-Chief/Associate Editor/Guest Editor for *[Journal name]* and was not involved in the editorial review or the decision to publish this article.

The authors declare the following financial interests/personal relationships which may be considered as potential competing interests:

Journal Pre-proof